Inorganic Chemistry

Article

pubs.acs.org/IC

Bis(imino)pyridine Iron Dinitrogen Compounds Revisited: Differences in Electronic Structure Between Four- and Five-Coordinate Derivatives.

S. Chantal E. Stieber,[†] Carsten Milsmann,[†] Jordan M. Hoyt,[†] Zoë R. Turner,[†] Kenneth D. Finkelstein,[‡] Karl Wieghardt,*[,⊥] Serena DeBeer,*[,§,⊥] and Paul J. Chirik*[,†]

[†]Department of Chemistry, Princeton University, Princeton, New Jersey 08544, United States

[‡]Cornell High Energy Synchrotron Source, Wilson Laboratory, Cornell University, Ithaca, New York 14853, United States

[§]Department of Chemistry and Chemical Biology, Baker Laboratory, Cornell University, Ithaca, New York 14853, United States

[⊥]Max-Planck Institute for Bioinorganic Chemistry, Stiftstrasse 34-36, D-45470 Mülheim an der Ruhr, Germany

Supporting Information

ABSTRACT: The electronic structures of the four- and five-coordinate aryl-substituted bis(imino)pyridine iron dinitrogen complexes, (^{iPr}PDI)FeN$_2$ and (^{iPr}PDI)Fe(N$_2$)$_2$ (^{iPr}PDI = 2,6-(2,6-^{i}Pr$_2$−C$_6$H$_3$−N=CMe)$_2$C$_5$H$_3$N), have been investigated by a combination of spectroscopic techniques (NMR, Mössbauer, X-ray Absorption, and X-ray Emission) and DFT calculations. Homologation of the imine methyl backbone to ethyl or isopropyl groups resulted in the preparation of the new bis(imino)pyridine iron dinitrogen complexes, (^{iPr}RPDI)FeN$_2$ (^{iPr}RPDI = 2,6-(2,6-^{i}Pr$_2$−C$_6$H$_3$−N=CR)$_2$C$_5$H$_3$N; R = Et, ^{i}Pr), that are exclusively four coordinate both in the solid state and in solution. The spectroscopic and computational data establish that the (^{iPr}RPDI)FeN$_2$ compounds are intermediate spin ferrous derivatives (S_{Fe} = 1) antiferromagnetically coupled to bis(imino)pyridine triplet diradical dianions (S_{PDI} = 1). While this ground state description is identical to that previously reported for (^{iPr}PDI)Fe(DMAP) (DMAP = 4-*N*,*N*-dimethylaminopyridine) and other four-coordinate iron compounds with principally σ-donating ligands, the d-orbital energetics determine the degree of coupling of the metal-chelate magnetic orbitals resulting in different NMR spectroscopic behavior. For (^{iPr}RPDI)Fe(DMAP) and related compounds, this coupling is strong and results in temperature independent paramagnetism where a triplet excited state mixes with the singlet ground state via spin orbit coupling. In the (^{iPr}RPDI)FeN$_2$ family, one of the iron singly occupied molecular orbitals (SOMOs) is essentially d_{z^2} in character resulting in poor overlap with the magnetic orbitals of the chelate, leading to thermal population of the triplet state and hence temperature dependent NMR behavior. The electronic structures of (^{iPr}RPDI)FeN$_2$ and (^{iPr}PDI)Fe(DMAP) differ from (^{iPr}PDI)Fe(N$_2$)$_2$, a highly covalent molecule with a redox noninnocent chelate that is best described as a resonance hybrid between iron(0) and iron(II) canonical forms as originally proposed in 2004.

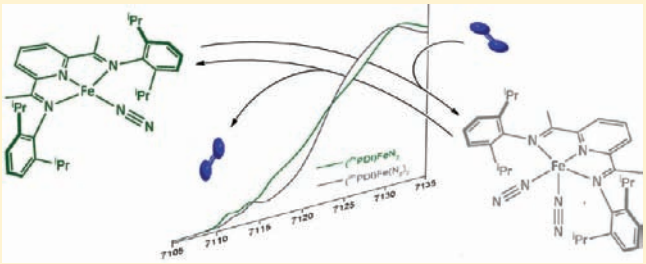

INTRODUCTION

Understanding the electronic structure of iron dinitrogen complexes is of fundamental and long-standing interest given the role of base metals as catalysts for industrial ammonia synthesis and their ubiquity in the active site in the nitrogenase family of enzymes.[1] Since Sacco and Aresta reported the synthesis of (Ph$_2$EtP)$_3$Fe(N$_2$)H$_2$ in 1968,[2] most isolated iron dinitrogen compounds contain weakly activated N$_2$ ligands that have proven resistant to subsequent functionalization chemistry.[1] Examples are known that yield hydrazine or ammonia upon treatment with mineral acids[3−6] and recent highlights include the synthesis and characterization of three-coordinate complexes with activated N$_2$ ligands,[7] ammonia synthesis using H$_2$ as the reductant,[8] N$_2$ cleavage and hydrogenation,[9] platforms that support relevant fixation intermediates,[10] and stoichiometric N$_2$ methylation[11] and silylation.[12]

Our laboratory has been exploring the chemistry of iron dinitrogen complexes in the context of base metal catalysis where the N$_2$ ligands serve as thermally labile leaving groups. Seeking to mimic the active species in Fe(CO)$_5$-catalyzed olefin hydrogenation,[13] isomerization, and hydrosilylation[14] under mild thermal conditions, we sought to prepare iron complexes with readily synthesized, modular π-accepting terdentate ligands. Aryl-substituted bis(imino)pyridines, popularized by Brookhart and Gibson in iron- and cobalt-catalyzed olefin polymerization,[15] seemed ideally suited for this purpose.[16] Sodium amalgam reduction of (^{iPr}PDI)FeCl$_2$ under an atmosphere of N$_2$ furnished the bis(imino)pyridine iron bis(dinitrogen) complex, (^{iPr}PDI)Fe(N$_2$)$_2$ (^{iPr}PDI = 2,6-

Received: December 22, 2011
Published: March 6, 2012

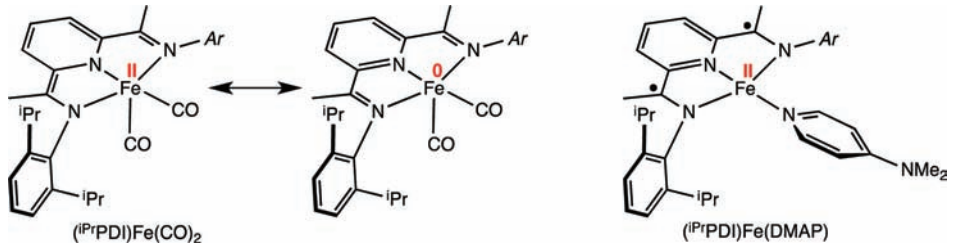

Figure 1. Electronic structures of (^{iPr}PDI)Fe(CO)$_2$ and (^{iPr}PDI)Fe(DMAP).

(2,6-^{i}Pr$_2$−C$_6$H$_3$−N=CMe)$_2$C$_5$H$_3$N).[17] Infrared and Mössbauer spectroscopies established that five-coordinate compound, (^{iPr}PDI)Fe(N$_2$)$_2$, is in equilibrium with the four-coordinate complex, (^{iPr}PDI)FeN$_2$ (eq 1).

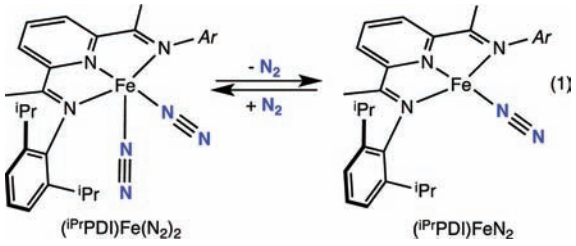

Gambarotta and co-workers have also synthesized a family of dinitrogen complexes derived from the bis(imino)pyridine iron dichloride, (^{iPr}PDI)FeCl$_2$.[18] Treatment of this compound with 3 equiv of NaH furnished an anionic iron dinitrogen compound where the bis(imino)pyridine has been deprotonated and the sodium is coordinated side-on to the terminal N$_2$ ligand. Increasing the number of equivalents of NaH used resulted in isolation and structural characterization of different anionic dinitrogen complexes with varying Na solvation and degrees of bis(imino)pyridine modification. This family of molecules demonstrates the ability of this ligand platform to support various types of N$_2$ compounds.

Investigations into the electronic structure of the five-coordinate (^{iPr}PDI)Fe(CO)$_2$ established a ground state distinct from (^{iPr}PDI)Fe(DMAP) (DMAP = 4-*N*,*N*-dimethylaminopyridine) and other four-coordinate neutral ligand complexes.[19−21] The former compound is a highly covalent molecule that can be described as either a low-spin iron(II) compound with a singlet (S_{PDI} = 0) dianionic chelate or as the formal iron(0) alternative with a neutral bis(imino)pyridine (Figure 1). The density functional theory (DFT) computed highest occupied molecular orbital (HOMO) is 68% chelate character with a large contribution from the iron center. On the basis of Jørgensen's original definition,[22] the bis(imino)pyridine is best classified as noninnocent as its spectroscopic oxidation state and that of the iron are ambiguous.[23]

Spectroscopic and computational studies on the seemingly related four-coordinate compound, (^{iPr}PDI)Fe(DMAP), established a diamagnetic ground state with an intermediate spin ferrous center (S_{Fe} = 1) antiferromagnetically coupled to a bis(imino)pyridine triplet diradical dianion (S_{PDI} = 1).[19] A low lying triplet state, likely derived from the spin isomer with a singlet chelate diradical (S_{PDI} = 0), mixes into the ground state giving rise to temperature independent paramagnetism. This phenomenon is evident in the ^{1}H NMR spectrum of (^{iPr}PDI)Fe(DMAP), where the resonances for the hydrogens in the plane of the iron center are significantly shifted from their diamagnetic reference values and do not shift with temperature (−80 to 80 °C). Throughout this work the term "diamagnetic reference values" refers to the chemical shifts of (^{iPr}PDI)Fe(CO)$_2$.[17,19] This behavior contrasts with the temperature dependent NMR spectroscopic behavior observed with (^{iPr}PDI)CoR (R = alkyl). This class of compounds is best described as low spin Co(II) derivatives antiferromagnetically coupled to a bis(imino)pyridine radical anion.[24] Thermal population of the low-lying triplet excited state accounts for the temperature dependent NMR behavior. In (^{iPr}PDI)Fe(DMAP) and the (^{iPr}PDI)CoR class of compounds, the bis(imino)pyridine is best described as redox-active[25−31] as there is no ambiguity in the oxidation state of either the metal centers or the chelate.

The difference in electronic structure between (^{iPr}PDI)Fe(CO)$_2$ and (^{iPr}PDI)Fe(DMAP) suggested that there may be similar differences between the four- and five-coordinate bis(imino)pyridine iron dinitrogen complexes. In a previous report from our laboratories, it was postulated that the structures of (^{iPr}PDI)Fe(N$_2$)$_2$ and (^{iPr}PDI)FeN$_2$ were the same based on the similarity of the Mössbauer isomer shifts (δ = 0.39 mm/sec, (^{iPr}PDI)Fe(N$_2$)$_2$; 0.38 mm/sec, (^{iPr}PDI)FeN$_2$) although computational studies were not performed to support the spectroscopic measurements. Several pieces of spectroscopic data indicate a possible difference between the electronic structures of the two iron bis(imino)pyridine dinitrogen compounds as well as the those of other four-coordinate bis(imino)pyridine iron neutral ligand complexes such as (^{iPr}PDI)Fe(DMAP). Applied field Mössbauer spectroscopy established significant differences in the values of the quadrupole splitting, indicating possible differences in d-orbital occupancies. In addition, the benzene-d_6 ^{1}H NMR spectrum of the equilibrium mixture of (^{iPr}PDI)Fe(N$_2$)$_2$ and (^{iPr}PDI)FeN$_2$ exhibits features distinct from both (^{iPr}PDI)Fe(CO)$_2$ and (^{iPr}PDI)Fe(DMAP). As noted previously,[21] the difference in chemical shift (absolute value) of the bis(imino)pyridine hydrogens that are in the plane of the iron are diagnostic of temperature independent paramagnetism and hence the electronic structure of the molecule. When strong field ligands are present, as in the case of (^{iPr}PDI)Fe(CO)$_2$ and (^{iPr}PDI)Fe(CN^{t}Bu)$_2$, the chemical shifts of the imine methyl groups, for example, appear at 2.08 and 2.31 ppm, respectively, and are close to their diamagnetic reference values. For four-coordinate neutral ligand complexes such as (^{iPr}PDI)Fe(DMAP), this resonance shifts upfield to −5.85 ppm and has only a modest temperature dependence. Similar values and temperature dependent phenomena have been observed with various neutral amine and ketone complexes.[21,32] By contrast, the imine methyl resonance of the equilibrium mixture of (^{iPr}PDI)Fe(N$_2$)$_2$ and (^{iPr}PDI)FeN$_2$ appears downfield in the vicinity of 14 ppm,[17] with the exact value depending on the temperature and the pressure of dinitrogen.

The synthesis and isolation of dimeric bis(imino)pyridine iron dinitrogen complexes bearing smaller 2,6-aryl substituents,

dx.doi.org/10.1021/ic202750n | *Inorg. Chem.* 2012, 51, 3770−3785

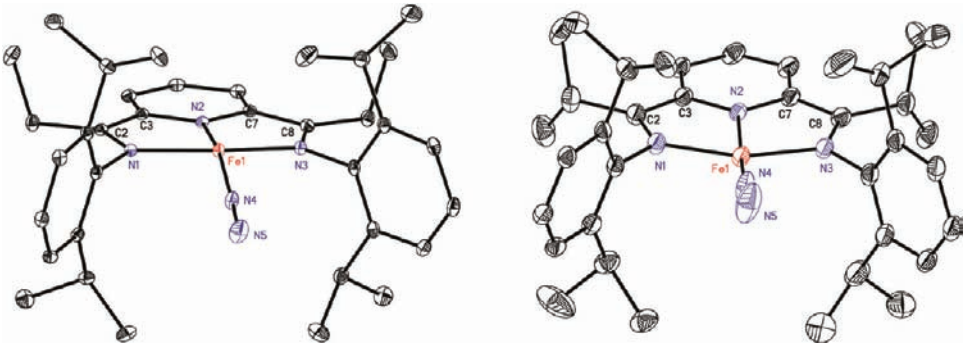

Figure 2. Representation of the solid state structures of (^{iPr}EtPDI)FeN_2 (left) and (^{iPr}iPrPDI)FeN_2 (right) at 30% probability ellipsoids. Hydrogen atoms omitted for clarity.

$[(^{R}PDI)Fe]_2(\mu_2\text{-}N_2)_2$ (^{R}PDI = 2,6-(2,6-R-C_6H_3–N=CMe)$_2C_5H_3N$; R = Me, Et) also raised questions about potential electronic structure differences between four- and five-coordinate N_2 compounds.[33] The benzene-d_6 ^{1}H NMR spectra of these compounds were reminiscent of the (^{R}PDI)-Fe(CO)$_2$ derivatives with imine methyl resonances at 1.78 (R = Me) and 1.65 ppm (R = Et). A full understanding of the electronic structure of these compounds is of particular interest given the performance of monomeric and dimeric bis(imino)-pyridine iron dinitrogen complexes in catalytic olefin hydrogenation[17,33–35] and hydrosilylation[17,36] as well as intra-[37] and intermolecular[38] [2π + 2π] cycloadditions and hydrogenative enyne and diyne cyclizations.[39]

Elucidation of the electronic structure of bis(imino)pyridine iron dinitrogen complexes and the influence of ligand substitution processes are critical in understanding fundamental transformations such as oxidative addition and metallocycle formation that comprise catalytic cycles. Here we describe the synthesis of new bis(imino)pyridine iron dinitrogen complexes that are exclusively four-coordinate as well as a more comprehensive experimental study of both the four- and five-coordinate derivatives by a combination of variable temperature NMR, Mössbauer, X-ray Absorption (XAS) and X-ray Emission (XES) spectroscopies. Full molecule and time dependent DFT calculations were also performed on both classes of compounds and augment the spectroscopic data.

RESULTS AND DISCUSSION

Synthesis of New Bis(imino)pyridine Iron Dinitrogen Complexes. The equilibrium mixture and rapid interconversion between (^{iPr}PDI)Fe(N_2)$_2$ and (^{iPr}PDI)FeN_2 in solution prompted subtle modification of the bis(imino)pyridine chelate architecture with the goal of favoring only one of the two species. Altering the substitution at the imine carbon was initially targeted as preservation of the 2,6-diisopropyl aryl groups was necessary to maintain monomeric iron dinitrogen compounds.[33] Gibson and co-workers have reported a straightforward method for the synthesis of bis(imino)pyridine iron dichlorides where the imine methyl groups have been homologated to ethyl and isopropyl substituents by a successive deprotonation-alkylation sequence.[40] Stirring either (^{iPr}EtPDI)-$FeCl_2$ or (^{iPr}iPrPDI)$FeCl_2$ (^{iPr}RPDI = 2,6-(2,6-$^{i}Pr_2$–C_6H_3–N=CR)$_2C_5H_3N$; R = Et, ^{i}Pr) with excess 0.5% sodium amalgam under a dinitrogen atmosphere for 15 min followed by filtration and recrystallization from pentane at −35 °C furnished the corresponding bis(imino)pyridine iron dinitrogen complexes (eq 2).

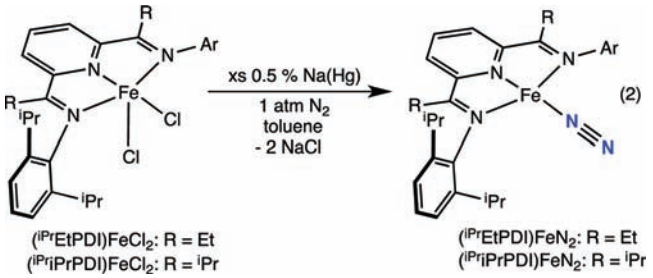

The short reaction times were critical as stirring the mixture longer over sodium amalgam resulted in formation of a bis(imino)pyridine iron arene compound where one of the diisopropyl aryl substituents is coordinated to the iron (see Supporting Information).[34]

Both complexes exhibit a single band assigned as an N≡N stretch in both the solid state and solution infrared spectra, consistent with four coordinate bis(imino)pyridine iron dinitrogen compounds. The pentane solution values of 2044 cm^{-1} and 2045 cm^{-1} for (^{iPr}EtPDI)FeN_2 and (^{iPr}EtPDI)FeN_2, respectively, are similar to the value of 2046 cm^{-1} reported for (^{iPr}PDI)FeN_2.[17] These bands shift to 2027 cm^{-1} in the solid state (KBr) spectrum of both compounds and indicate that an additional N_2 ligand does not coordinate upon isolation in the solid state.

The solid state structures of both (^{iPr}EtPDI)FeN_2 and (^{iPr}iPrPDI)FeN_2 were determined by X-ray diffraction and representations of the molecules are presented in Figure 2. Selected bond distances and angles are reported in Table 1. The crystallographic data clearly establish the formation of four-coordinate bis(imino)pyridine iron dinitrogen complexes, consistent with the solution and solid state infrared data. For (^{iPr}EtPDI)FeN_2, the dinitrogen ligand is lifted slightly out of the idealized metal-bis(imino)pyridine chelate plane as evidenced by the N(2)–Fe(1)–N(4) angle of 163.29(6)°. This distortion is slightly less pronounced in (^{iPr}iPrPDI)FeN_2 where this angle is 169.42(16)°. The bond distortions of the chelate, an established reporter of bis(imino)pyridine oxidation state,[30] are consistent with two electron reduction and therefore ferrous compounds (Table 1).

Because the ^{1}H NMR chemical shifts of the in-plane bis(imino)pyridine hydrogens provide insight into the electronic structure, variable temperature experiments were conducted with toluene-d_8 solutions of (^{iPr}EtPDI)FeN_2 and (^{iPr}iPrPDI)FeN_2. A summary of the measured chemical shifts of the in-plane hydrogens as a function of temperature is reported in Table 2 (see also Supporting Information, Tables S1–S2). Also included in Table 2 are the corresponding shifts for the

dx.doi.org/10.1021/ic202750n | Inorg. Chem. 2012, 51, 3770–3785

Table 1. Selected Bond Distances (Å) and Angles (deg) for (^{iPr}EtPDI)FeN$_2$ and (^{iPr}iPrPDI)FeN$_2$

	(^{iPr}EtPDI)FeN$_2$	(^{iPr}iPrPDI)FeN$_2$
Fe(1)−N(1)	1.9121(12)	1.914(3)
Fe(1)−N(2)	1.8423(12)	1.842(3)
Fe(1)−N(3)	1.9114(12)	1.904(3)
Fe(1)−N(4)	1.8171(14)	1.799(3)
N(4)−N(5)	1.112(2)	1.117(5)
N(1)−C(2)	1.3420(19)	1.344(4)
N(3)−C(8)	1.341(2)	1.342(4)
N(2)−C(3)	1.3728(18)	1.370(4)
N(2)−C(7)	1.3724(18)	1.372(4)
C(2)−C(3)	1.427(2)	1.440(5)
C(7)−C(8)	1.431(2)	1.432(5)
N(1)−Fe(1)−N(2)	80.46(5)	80.82(11)
N(1)−Fe(1)−N(3)	160.27(5)	160.71(12)
N(1)−Fe(1)−N(4)	97.64(6)	98.81(13)
N(2)−Fe(1)−N(3)	80.43(5)	80.64(11)
N(2)−Fe(1)−N(4)	163.29(6)	169.42(16)
N(3)−Fe(1)−N(4)	99.24(6)	98.44(13)

Table 2. Chemical Shifts of in Plane Bis(imino)Pyridine Hydrogens As a Function of Temperature[a]

resonance	T (°C)	(^{iPr}EtPDI)FeN$_2$	(^{iPr}iPrPDI)FeN$_2$	(^{iPr}PDI)FeN$_2$[d]
imine CH$_X$[b]	−40	2.21	3.55	3.8
	−20	3.59	3.76	6.99
	0	5.62	4.03	11.68
	20	8.62	4.31	16.26
	40	11.53	4.6	20.67
	60	14.23	4.91	24.88
p-pyridine	−40	7.34	ND[c]	6.47
	−20	6.58	4.48	5.43
	0	5.05	1.82	3.46
	20	2.93	−0.72	2.31
	40	0.75	−2.87	−0.32
	60	ND[c]	−4.81	−2.1
m-pyridine	−40	8.31	8.92	9.08
	−20	8.65	9.72	9.43
	0	9.37	10.7	10.02
	20	10.3	11.49	10.55
	40	10.96	12.1	11.03
	60	11.51	12.61	11.45

[a]Spectra recorded in toluene-d_8 under 1 atm of N$_2$. Additional NMR spectroscopic data are reported in the Supporting Information, Tables S1 and S2. [b]x = 1 for (^{iPr}iPrPDI)FeN$_2$; x = 2 for (^{iPr}EtPDI)FeN$_2$; x = 3 for (^{iPr}PDI)FeN$_2$. [c]Not determined because of overlapping resonances. [d]For the equilibrium (^{iPr}PDI)Fe(N$_2$)$_2$/(^{iPr}PDI)FeN$_2$.

equilibrium mixture of (^{iPr}PDI)FeN$_2$ and (^{iPr}PDI)Fe(N$_2$)$_2$ as a function of temperature.

For both pure four-coordinate bis(imino)pyridine iron dinitrogen complexes, the temperature dependence of the chemical shifts is profound. Because there is no evidence that (^{iPr}EtPDI)FeN$_2$ and (^{iPr}iPrPDI)FeN$_2$ coordinate additional dinitrogen, the origin of the temperature dependence is a result of the electronic structure rather than a chemical equilibrium involving ligand coordination and dissociation. For both compounds, the *p*-pyridine resonance appears close to its diamagnetic reference value at −40 °C and then shifts upfield upon warming. In the case of (^{iPr}iPrPDI)FeN$_2$, this value appears upfield of SiMe$_4$ at −4.81 ppm at 60 °C. An opposite trend was observed for the *m*-pyridine protons where values close to those expected for a diamagnetic compound were obtained at low temperature that then shift *downfield* upon warming.

The chemical shift of the hydrogen attached to the imine position is also temperature dependent, the extent of which is determined by the specific compound and the degree of alkylation. For (^{iPr}PDI)FeN$_2$ this effect is the most pronounced as the imine methyl group shifts from −3.80 ppm at −40 °C to 24.88 ppm upon warming to 60 °C. This downfield shift is most likely not due to additional N$_2$ coordination as increased concentration of (^{iPr}PDI)Fe(N$_2$)$_2$ would shift the resonance upfield toward the diamagnetic reference value. A similar downfield shift of the imine methylene resonance was also observed upon increasing the temperature of toluene-d_8 solutions of (^{iPr}EtPDI)FeN$_2$, albeit slightly less pronounced than with (^{iPr}PDI)FeN$_2$. For the ethylated derivative, the imine methylene appears at 14.23 ppm at 60 °C. In keeping with this trend, the imine methine hydrogens are the least temperature sensitive of the three iron dinitrogen compounds examined appearing only slightly downfield at 4.91 ppm at 60 °C.

The temperature dependence of the ^{1}H NMR chemical shifts clearly rules out temperature independent paramagnetism found in neutral ligand complexes with principally σ-donating ligands such as (^{iPr}PDI)Fe(DMAP) and establishes distinct electronic structures for the (^{iPr}RPDI)FeN$_2$ class of compounds. The most likely explanation for the observed NMR behavior is thermal population of a low-lying paramagnetic excited state. This phenomenon was first identified in bis(imino)pyridine chemistry by Budzelaar and co-workers for the (^{R}PDI)CoR class of compounds[24,41] and later verified by our laboratory with the spin crossover behavior of alkyl-substituted bis(imino)pyridine cobalt halide complexes.[42] The temperature dependence of the chemical shifts of the (^{iPr}RPDI)FeN$_2$ compounds is more dramatic than the cobalt alkyls suggesting a more energetically accessible triplet state. The chemical shift dispersion as a function of temperature is likely a result of the singlet−triplet gap. Because (^{iPr}iPrPDI)-FeN$_2$ exhibits the least temperature dependent shifts, the triplet state appears the least energetically accessible in the series. The origin of this effect is not understood presently.

Mössbauer Spectroscopic Studies. The isolation of pure four coordinate bis(imino)pyridine iron dinitrogen complexes provided the opportunity to study these compounds by zero-field ^{57}Fe Mössbauer spectroscopy. Representative spectra for (^{iPr}EtPDI)FeN$_2$ and (^{iPr}iPrPDI)FeN$_2$ recorded at 80 K are presented in Figure 3. The isomer shift (δ) for both compounds is 0.37 mm/sec with quadrupole splittings (ΔE_Q) of 1.75 (Et) and 1.85 mm/sec (^{i}Pr). These values are consistent with those previously reported for (^{iPr}PDI)FeN$_2$ (δ = 0.38 mm/sec; ΔE_Q = +1.72 mm/sec), suggesting similar electronic structures for the four-coordinate species. Applied field Mössbauer studies were previously reported for (^{iPr}PDI)FeN$_2$ and (^{iPr}PDI)Fe(N$_2$)$_2$,[19] and variable temperature zero-field studies on both compounds did not show any significant changes in δ or ΔE_Q between 80 and 295 K.

X-ray Absorption Studies of Bis(imino)pyridine Iron Dinitrogen Complexes. To further elucidate the electronic structures of the four- versus five-coordinate bis(imino)pyridine iron dinitrogen compounds and to distinguish these complexes from previously reported compounds with principally σ-donating ligands such as (^{iPr}PDI)Fe(DMAP), selected com-

dx.doi.org/10.1021/ic202750n | Inorg. Chem. 2012, 51, 3770−3785

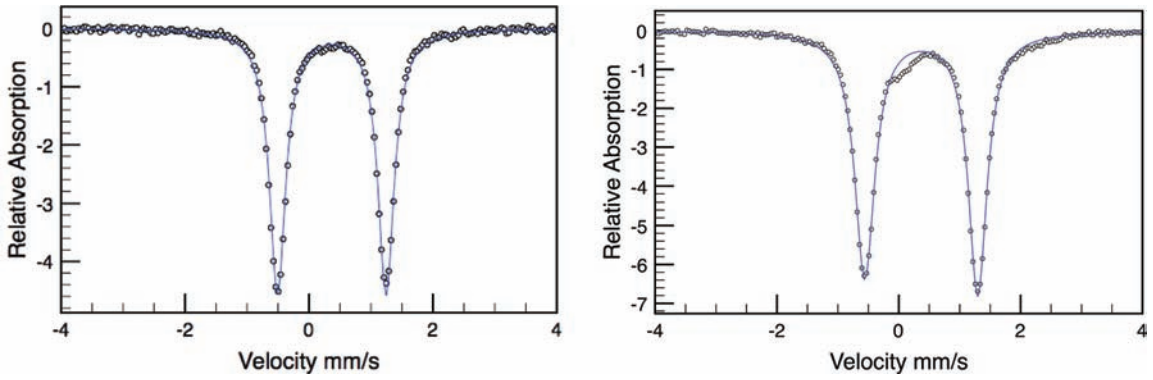

Figure 3. Zero-field ^{57}Fe Mössbauer spectra for (^{iPr}EtPDI)FeN_2 (left, δ = 0.37 mm/sec, $|\Delta E_Q|$ = 1.75 mm/sec) and (^{iPr}iPrPDI)FeN_2 (right, δ = 0.37 mm/sec, $|\Delta E_Q|$ = 1.85 mm/sec) recorded at 80 K.

pounds were studied by X-ray Absorption Spectroscopy (XAS). This technique provides insight into the oxidation state of the metal absorber,[43] local site symmetry, and coordination environment.[43−45] In a simplified model, it involves the excitation of a metal 1s electron into empty valence orbitals. In iron compounds, the first observed transition, or pre-edge, has been shown to shift by approximately one electronvolt (eV) per one electron oxidation, making it a useful technique for assessing metal oxidation states.[45] This method has previously been applied to understand the electronic structure of bis(imino)pyridine compounds and here, it is utilized again to obtain further insight into the oxidation state and coordination environment of the iron center.[46]

The normalized XAS data for (^{iPr}PDI)$FeCl_2$, (^{iPr}PDI)Fe$(CO)_2$, and (^{iPr}PDI)Fe(DMAP)[46] are presented in Figure 4. This set of reference compounds was selected to span a range of coordination and metal/ligand oxidation states within the bis(imino)pyridine iron framework. (^{iPr}PDI)$FeCl_2$ is an established five-coordinate, high spin ferrous compound with a neutral ligand, whereas (^{iPr}PDI)Fe(DMAP) is a four-coordinate intermediate spin ferrous derivative with a diradical bis(imino)pyridine chelate.[19] The iron dicarbonyl complex, (^{iPr}PDI)Fe$(CO)_2$, provides an example of a five-coordinate compound with a high degree of covalency and a redox noninnocent chelate.[19,20] Also highlighted in Figure 4 (bottom) are spectra for the four- and five-coordinate bis(imino)pyridine iron dinitrogen compounds, (^{iPr}PDI)FeN_2 and (^{iPr}PDI)Fe$(N_2)_2$. In addition, variable temperature XAS measurements were performed on samples of (^{iPr}PDI)FeN_2 to determine whether or not the temperature effects observed by ^{1}H NMR spectroscopy would also be manifest in the solid state. No appreciable changes in the spectra were observed (see Supporting Information, Figure S2).

Although these compounds rapidly interchange in solution, each can be obtained in approximately 95% purity (as judged by infrared and Mössbauer spectroscopy) in the solid state by using the appropriate isolation techniques. Recrystallization of the mixture under a dinitrogen atmosphere at −35 °C furnished (^{iPr}PDI)Fe$(N_2)_2$ while exposure of the sample to vacuum enriches the four coordinate compound, (^{iPr}PDI)FeN_2.[17,19,21] Following XAS data collection, the integrity of the sample was assessed by infrared spectroscopy. No observable differences were detected in the IR spectra.

The edge (∼7117−7130 eV) for (^{iPr}PDI)$FeCl_2$ is typical of a high-spin Fe(II) coordination compound,[45] and sets a baseline for determining the spectral properties of a five-coordinate

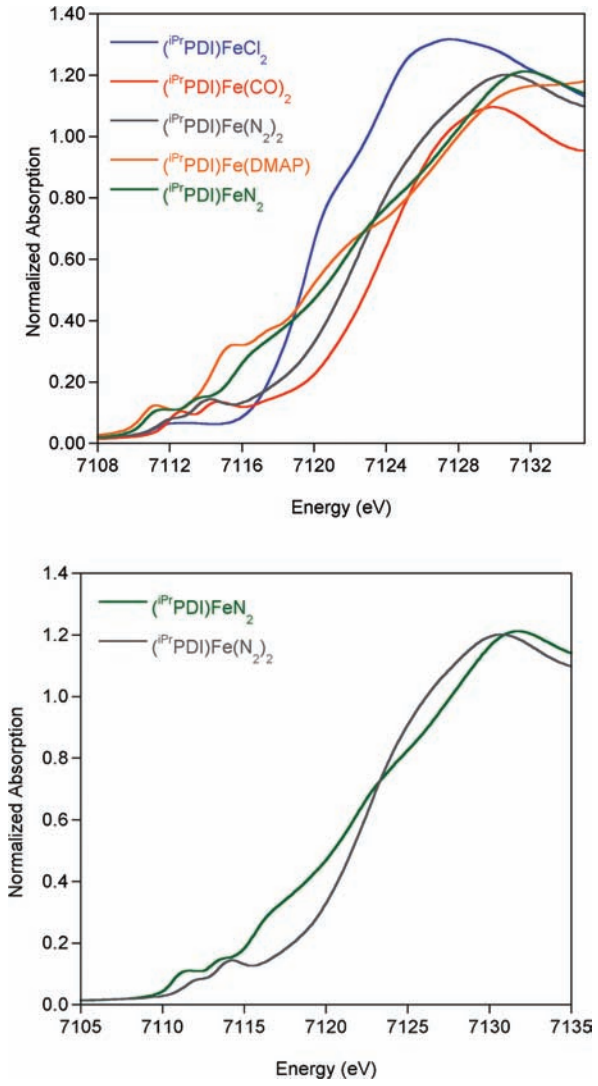

Figure 4. Normalized Fe K-edge X-ray absorption spectra of bis(imino)pyridine iron compounds. Data collected at 10 K.

species with a neutral, redox innocent bis(imino)pyridine. By comparison, the edge for a related five-coordinate compound, (^{iPr}PDI)Fe$(CO)_2$, is shifted to higher energy by 4.4 eV. This is attributed to the strong backbonding to the carbonyl ligands, which results in the appearance of a more highly oxidized center.[47] The shape of the edge for (^{iPr}PDI)Fe$(N_2)_2$ is almost

dx.doi.org/10.1021/ic202750n | Inorg. Chem. 2012, 51, 3770−3785

identical to that of (^{iPr}PDI)Fe(CO)$_2$, and supports a similar electronic structure and coordination environment; however, it is shifted by 1.3 eV to lower energy, likely because of the weaker π-backbonding to N_2. The rising edge (~7113−7117 eV) of (^{iPr}PDI)FeN_2 and (^{iPr}PDI)Fe(DMAP) both appear at lower energy than the 5-coordinate complexes. This may reflect the decreased coordination number in these complexes, which may lower the energy of the 1s to 4p$_z$ transition. However, we note that the interpretation of the rising edge is greatly complicated by numerous features superimposed on the rising edge. Analogous features have been observed for ferrocene,[48,49] ferricyanide,[45] and heme complexes,[50] and have been attributed to 1s to 4p plus ligand to metal charge transfer "shakedown" transitions,[51] or alternatively an iron 1s to ligand π^* transition. For the bis(imino)pyridine family of compounds, an iron 1s to ligand π^* transition is a likely candidate because of the strong π-accepting nature of the ^{iPr}PDI ligand. Similar effects have been observed in Mn and Cr centers bound to extended π systems.[52] Hence, we tentatively assign the features in the 7112.5−7115.5 eV region as 1s to ligand π^* transitions. This assignment is further discussed in the computational section of this paper. We note that the higher energy features, which are not predicted within a time-dependent DFT (TD-DFT) model (i.e., above 7115.5 eV), may arise from charge transfer processes.

To quantify the changes in these spectral features, the pre-edge and rising edge data were modeled using pseudo-Voigt peaks.[53] The lowest energy peaks, or pre-edge features, correspond dominantly to 1s to 3d features, and the higher energy rising edge features are likely 1s to ligand π^* features as discussed above. Both features may gain intensity through symmetry-mediated 4p mixing, giving the transition electric dipole allowed character.

The fit results are summarized in Table 3. The pre-edge positions for (^{iPr}PDI)Fe(DMAP) (7111.1 eV) and (^{iPr}PDI)-FeN_2 (7111.4 eV) appear to the lowest energies in the series, and also have the largest intensities (10.4(2), 17.2(2), respectively). For (^{iPr}PDI)FeCl_2, (^{iPr}PDI)Fe(CO)$_2$, and (^{iPr}PDI)Fe(N_2)$_2$ the first pre-edge features all appear to higher energies (7111.8(1) eV, 7112.5 eV, 7111.9 eV, respectively) and with lower intensities (6(2), 7.9, 5.0, respectively). These are consistent with iron(II) oxidation states, although this assignment may be complicated by backbonding to the CO ligands, in the case of (^{iPr}PDI)Fe(CO)$_2$. This will be further discussed in the Computational Section. The lower energy 1s to 3d features for the four-coordinate compounds are consistent with reduced ligand-field strengths (as compared to the five-coordinate complexes), which lowers the overall d-manifold energies. The lower intensities for the four-coordinate compounds are also related to the lower coordination number, and specifically derive from higher centro-symmetry, resulting in a decrease in 3d-4p mixing.[43]

Table 3. Experimentally Fit XAS Pre-Edge Positions and Areas[a]

	(^{iPr}PDI)FeCl_2	(^{iPr}PDI)Fe(CO)$_2$	(^{iPr}PDI)Fe(N_2)$_2$	(^{iPr}PDI)Fe(DMAP)	(^{iPr}PDI)FeN_2
peak 1 (eV)	7111.8	7112.4	7111.9	7111.1	7111.3
peak 1 int. (W)	6(2)	7.9	5.0	10.4(2)	17.2(2)
peak 1 int. (S)	8(3)	10.2(1)	6.4(1)	13.3(3)	22.0(2)
peak 2 (eV)	7113.5(3)	7114.5	7114.0	7115.0	7113.3
peak 2 int. (W)	7(3)	12.9(2)	15.5(1)	15.7(9)	12.8(4)
peak 2 int. (S)	8(4)	16.6(2)	19.8(4)	20.2(1)	16.3(5)
average M−L bond length (Å)	2.200[b]	1.865[c]	1.889[d]	1.912[c]	NA

[a]Intensities denoted with a (W) were simulated using the method reported by Westre et al.,[45] and those denoted with an (S) were simulated using the Simpson's Rule method.[56] All intensities are multiplied by a factor of 100. Errors are listed in parentheses. Those that are less <1 are below experimental resolution and therefore omitted. [b]Data taken from ref 15a. [c]Data taken from ref 19. [d]Data taken from ref 17.

In addition to the pre-edge features, the rising edge features were also fit. As these features are not as well resolved as the pre-edge, there are larger errors in the fit intensities. In any case, the energies and general intensity trends still provide useful insight. For (^{iPr}PDI)Fe(CO)$_2$ and (^{iPr}PDI)Fe(N_2)$_2$ the Fe 1s to ligand π^* features appear at 7114.5 and 7114.0 eV, respectively, with the higher energy shift for (^{iPr}PDI)Fe(CO)$_2$ likely attributed to CO backbonding. The relative shapes and intensities of the rising edge features, however, are similar, which suggests related overall electronic environments. For (^{iPr}PDI)FeN_2, the rising edge features are shifted relative to those of (^{iPr}PDI)Fe(DMAP), with the first being at 7113.3 eV, 7115.0 eV, respectively. The 1.7 eV shift to higher energy for (^{iPr}PDI)Fe(DMAP) suggests that these two compounds do not have exactly the same electronic structures and the assignments and origins of these transitions will be further discussed in the Computational Section.

X-ray Emission Studies of Bis(imino)pyridine Iron Dinitrogen Complexes. X-ray Emission Spectroscopy (XES) has also recently found application in transition metal chemistry as it provides useful information about ligand identity, metal−ligand bonding, and metal spin state.[54,55] The experiment involves the detection of the emission of photons (electron decay) following the ionization of an Fe-1s electron.[57] There are three features of an XES spectrum that contain the most relevant chemical information: the Kβ' and K$\beta_{1,3}$ lines resulting from an electric dipole allowed 3p to 1s transition,[58] and the K$\beta_{2,5}$ and Kβ'' lines (or valence to core region, V2C) arising from a valence electron (ligand np or ns) to metal 1s transition.[59,60] The K$\beta_{1,3}$ (main line, ~7030−7080 eV) region is dominated by 3p-3d exchange correlation with some contribution from 3p spin−orbit coupling, resulting in sensitivity toward spin state, but little sensitivity toward ligand identity.[58] A recent study with a family of iron coordination compounds, augmented with DFT calculations, has demonstrated that the V2C region (~7080−7120 eV) is relatively insensitive to changes in the Fe site symmetry, but changes in spin state and ligand identities have significant contributions to the intensities and energy distributions.[58]

The Kβ main line in the XES spectrum of (^{iPr}PDI)FeCl_2 (Figure 5, left) exhibits a Kβ' feature at 7057.8(2) eV, in agreement with the established high spin state for the compound.[19,61] Similarly, the high energy of the K$\beta_{1,3}$ transition at 7060.3 eV, establishes a reference for a high spin bis(imino)pyridine iron(II) derivative, and is within the range of previously reported K$\beta_{1,3}$ positions for tetrahedral and octahedral high spin iron(II) coordination compounds.[54] On going to (^{iPr}PDI)Fe(CO)$_2$, the Kβ' feature is absent and the mainline appears to lower energy (7058.6 eV), which is consistent with a low-spin ferrous species.[54] Similarly, for

dx.doi.org/10.1021/ic202750n | Inorg. Chem. 2012, 51, 3770−3785

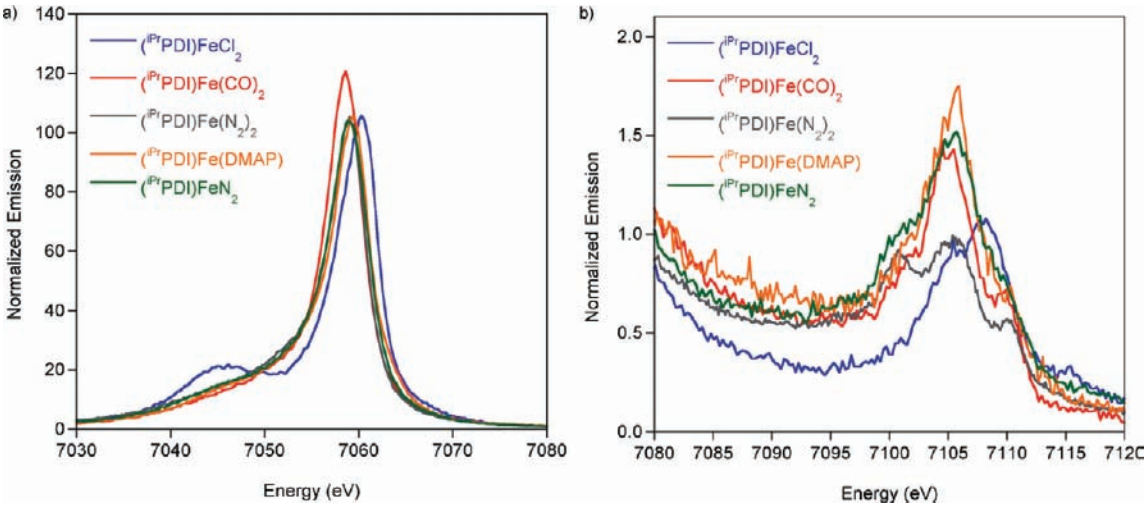

Figure 5. (a) Kβ main line and (b) valence to core XES spectra for (^{iPr}PDI)Fe compounds highlighting the paramagnetism of (^{iPr}PDI)$FeCl_2$ as compared to the diamagnetism of the other compounds. The spectra of (^{iPr}PDI)FeN_2 and (^{iPr}PDI)$Fe(N_2)_2$ overlay in the Kβ main line.

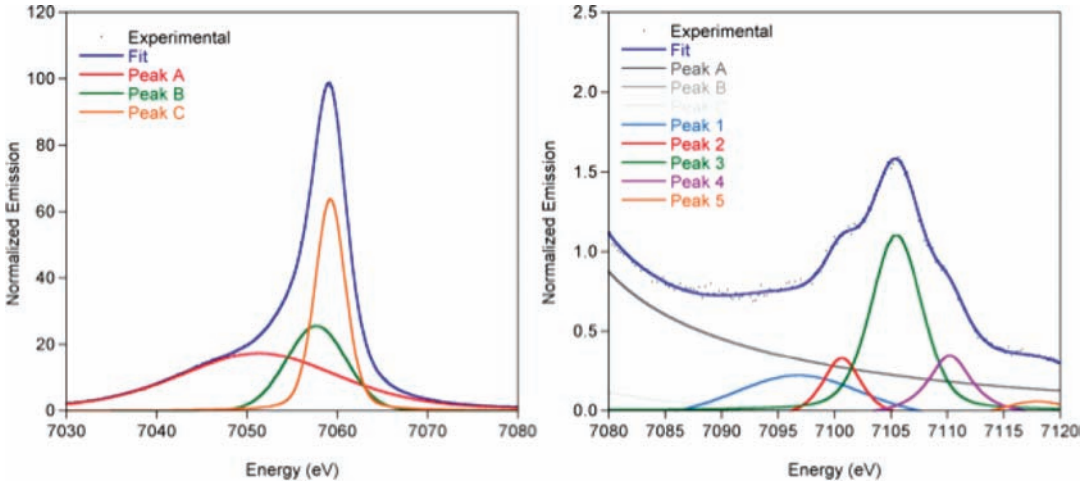

Figure 6. Representative fit of (^{iPr}PDI)FeN_2 using five peaks to model the V2C.

Table 4. Parameters from Fits to Experimental XES of Main Line and V2C Using 5 Peaks to Model the V2C[a]

	(^{iPr}PDI)$FeCl_2$	(^{iPr}PDI)$Fe(CO)_2$	(^{iPr}PDI)$Fe(N_2)_2$	(^{iPr}PDI)Fe(DMAP)	(^{iPr}PDI)FeN_2
K$\beta_{1,3}$ (eV)	7060.4	7058.6	7059.1	7059.4	7059.2
Kβ' (eV)	7048.5	7051.4(6)	7051.0	7048.9(2)	7051(2)
peak 1 (eV)	7100(1)	7096.0(6)	7095.8(7)	7095.5	7096.9(5)
peak 1 int.[b]	0.27(7)	0.27(4)	0.25(6)	0.25(0)	0.27(5)
peak 2 (eV)	7105.2(2)	7101.0	7100.7(4)	7101.6	7100.8(2)
peak 2 int.[b]	0.21(6)	0.18(2)	0.27(4)	0.17(0)	0.14(3)
peak 3 (eV)	7108.7	7105.2	7105.6	7105.5	7105.4
peak 3 int.[b]	0.36(4)	0.40(3)	0.38(5)	0.36(0)	0.38(4)
peak 4 (eV)	7118.5(5)	7114.2(1)	7115.2(5)	7113.5	7114.4(5)
peak 4 int.[b]	0.16(2)	0.15(1)	0.10(0)	0.22(0)	0.21(2)
peak 5 (eV)	7122(1)	7118.0	7123.0	7118.0	7118.0
# of fits	20	12	15	28	18

[a]Errors are listed in parentheses. Errors <1 are not listed. [b]Intensities are taken to be a fraction of 1. Where 1 = V2C area = SUM(peaks 1:4).

(^{iPr}PDI)$Fe(N_2)_2$, (^{iPr}PDI)Fe(DMAP) and (^{iPr}PDI)FeN_2, only a single Kβ main line feature is observed. The absence of the Kβ' feature in all of these complexes is consistent with overall $S = 0$ diamagnetic systems. In all cases, the energies fall at 7059.2 ± 0.2 eV, and thus, in addition to the absence of the Kβ' feature, are also too low in energy to be assigned as high spin complexes. It is also of interest to note that the Kβ main line of (^{iPr}PDI)$Fe(CO)_2$ appears ~0.8 eV lower in energy than all the other low spin PDI complexes. This may be a contribution from backbonding, and parallels the trends observed for $[Fe(CN)_6]^{4-}$ relative to $[Fe(tacn)_2]^{2+}$.[54] Finally, we note, that the impact of metal ligand coupling on Kβ mainline spectra is

dx.doi.org/10.1021/ic202750n | Inorg. Chem. 2012, 51, 3770–3785

Table 5. Comparison of Experimentally and Computationally Determined Geometric Parameters for (^{iPr}PDI)Fe(N_2)$_2$ and (^{iPr}PDI)FeN_2

	(^{iPr}PDI)Fe(N_2)$_2$			(^{iPr}PDI)FeN_2		
	exp.	RKS	BS(1,1)	exp.[a]	RKS	BS(2,2)
Fe(1)−N(1)	1.945	2.008	2.025	1.914	1.973	1.953
Fe(1)−N(2)	1.836	1.834	1.875	1.842	1.827	1.885
Fe(1)−N(3)	1.947	2.001	2.019	1.904	1.970	1.953
Fe(1)−N(4)	1.834	1.876	1.861	1.799	1.823	1.837
Fe(1)−N(6)	1.880	1.827	1.917			
N(1)−C(2)	1.333	1.330	1.327	1.344	1.327	1.349
N(2)−C(3)	1.379	1.381	1.371	1.370	1.378	1.366
N(2)−C(7)	1.377	1.381	1.372	1.372	1.378	1.366
N(3)−C(8)	1.334	1.332	1.329	1.341	1.327	1.350
C(2)−C(3)	1.428	1.436	1.445	1.439	1.441	1.440
C(7)−C(8)	1.427	1.435	1.443	1.432	1.441	1.439
N(4)−N(5)	1.089	1.105	1.107	1.116	1.111	1.110
N(6)−N(7)	1.104	1.108	1.106			
N(2)−Fe(1)−N(4)				169.42	155.79	178.82

[a]From (^{iPr}iPrPDI)Fe(N_2).

not yet fully understood, and investigations of these effects are underway in our laboratory.

The V2C XES data for the five (^{iPr}PDI)Fe complexes are shown in Figure 5. For (^{iPr}PDI)FeCl_2 the V2C XES is shifted to higher energy, 7108.7 eV, as compared to the other compounds and also appears to have a lower overall intensity. The lower intensity can be attributed to a higher spin state resulting in longer metal−ligand bonds, and decreased iron p mixing. The V2C region of all the diamagnetic compounds is highly structured, with three primary features at similar positions for all compounds (7101, 7105, 7113 eV). Where these spectra differ, however is in the relative intensities of these features. For (^{iPr}PDI)Fe(N_2)$_2$, the relative intensities of the first and second features (7101, 7105 eV) are approximately equal, whereas in the other diamagnetic compounds the feature at 7101 eV has a lower intensity relative to the 7105 eV feature. The 7101 eV feature is therefore attributed to non-PDI ligand coordination, and appears to be able to differentiate between the four- and five-coordinate N_2 compounds. This is consistent with the shape of the V2C spectrum of the four-coordinate reference compound, (^{iPr}EtPDI)FeN_2, in which the 7101 eV feature also has a lower relative intensity (see Supporting Information, Figure S3).

To further quantify the spectral contributions, the data were fit using BlueprintXAS (Figure 6, Table 4).[62−64] The V2C region was modeled by both five- and six-peak fits (Tables 4, and Supporting Information, Figures S4−S13 and Table S3, respectively). For (^{iPr}PDI)Fe(N_2)$_2$ Peak 2 is more intense, 0.27(4), than for (^{iPr}PDI)FeN_2, 0.14(3), which is attributed to additional N_2 coordination. Similarly, Peak 3 is less intense for (^{iPr}PDI)Fe(CO)$_2$, 0.15(1), and (^{iPr}PDI)Fe(N_2)$_2$, 0.10(0), as compared to the other compounds supporting similar electronic structures and bonding environments for these two compounds. These results suggest that the V2C region is able to distinguish between four- and five-coordinate nitrogen environments in (^{iPr}PDI)Fe compounds, and will be further examined in the Computational Section.

Computational Studies: (^{iPr}PDI)Fe(N_2)$_2$ and (^{iPr}PDI)-FeN_2. Full molecule DFT (B3LYP) calculations on both (^{iPr}PDI)Fe(N_2)$_2$ and (^{iPr}PDI)FeN_2 were performed. For (^{iPr}PDI)Fe(N_2)$_2$, three different computational models were used to explore the experimentally determined diamagnetic ground state. In analogy to the isoelectronic compound (^{iPr}PDI)Fe(CO)$_2$, which has been previously shown to possess a highly covalent, closed-shell singlet ground state,[19,20] calculations were initially performed using a spin-restricted approach (RKS). To account for a possible open-shell singlet ground state, similar to that described for (^{iPr}PDI)Fe-(DMAP),[19] a spin-unrestricted broken-symmetry (BS) model was also investigated. Because the experimentally determined bond lengths of the PDI ligand in (^{iPr}PDI)Fe(N_2)$_2$ lie between the accepted values for [PDI$^-$] and [PDI^{2-}], two different broken-symmetry approaches, BS(1,1) and BS(2,2), were studied. These correspond to the electronic ground states (^{iPr}PDI$^-$)Fe^{I}(N_2)$_2$ and (^{iPr}PDI^{2-})Fe^{II}(N_2)$_2$, respectively. Note that the former electronic structure description contains a low spin Fe^{I} center (d^7, S_{Fe} = 1/2) and a PDI$^-$ radical (S_{PDI} = 1/2) while the latter contains an intermediate-spin Fe^{II} ion (d^6, S_{Fe} = 1) and a triplet diradical dianion (S_{PDI} = 1). In both cases antiferromagnetic coupling between the ligand and the metal center accounts for the diamagnetic ground state.

Geometry optimizations at the B3LYP level of DFT were performed for all three models and produced two different solutions. The two broken-symmetry approaches converged to the same BS(1,1) solution. A comparison of the total energies showed that the BS(1,1) solution is only 2.4 kcal/mol more stable than the RKS solution. The geometric parameters of both the RKS and the BS(1,1) solutions are in excellent agreement with the crystallographic data (Table 5). Even though the RKS solution shows slightly better agreement in the metal−ligand and intraligand bond distances, the parameters obtained from the BS(1,1) solution are within the generally accepted error range for DFT geometry optimizations.[65] Therefore, neither solution can be excluded based on structural or energetic arguments.

dx.doi.org/10.1021/ic202750n | Inorg. Chem. 2012, 51, 3770−3785

In an attempt to distinguish the two possible (^{iPr}PDI)Fe(N_2)$_2$ models, ^{57}Fe Mössbauer parameters were computed. The calculation of Mössbauer parameters has been shown to be a reliable method to calibrate computational results against experiment and to evaluate different electronic structures.[66] While both the isomer shift and the quadrupole splitting obtained via the RKS approach (δ = 0.38 mm/s, ΔE_Q = −0.65 mm/s) are in excellent agreement with the experimental values (δ = 0.39 mm/s, ΔE_Q = −0.53 mm/s), the values provided by the BS(1,1) model are less accurate (δ = 0.51 mm/s, ΔE_Q = −0.81 mm/s). In particular the isomer shift is outside the generally accepted range.[66] On the basis of these results, the electronic structure of (^{iPr}PDI)Fe(N_2)$_2$ is best described as a closed-shell singlet with (^{iPr}PDI^{2-})Fe^{II}(N_2)$_2$ and (^{iPr}PDI^0)-Fe^0(N_2)$_2$ resonance structures, similar to the electronic structure description posited for (^{iPr}PDI)Fe(CO)$_2$.[19,20] Note that both ligand and metal are in their singlet states (S = 0) in both resonance structures. Notably, the HOMO contains 35% iron and 58% pyridine diimine ligand character supporting the high covalency in the metal ligand π interaction. This is again similar to the HOMO of (^{iPr}PDI)Fe(CO)$_2$, which contains 68% ligand character.[19] A qualitative molecular orbital diagram of (^{iPr}PDI)Fe(N_2)$_2$ is presented in Figure 7. This electronic structure description was originally proposed in 2004 with the original synthesis of the compound[17] and, based on NMR chemical shift data, is also appropriate for the dimeric bis(imino)pyridine iron dinitrogen compounds, [(^{R}PDI)-FeN_2]$_2$(μ-N_2) (R = Me, Et).[33]

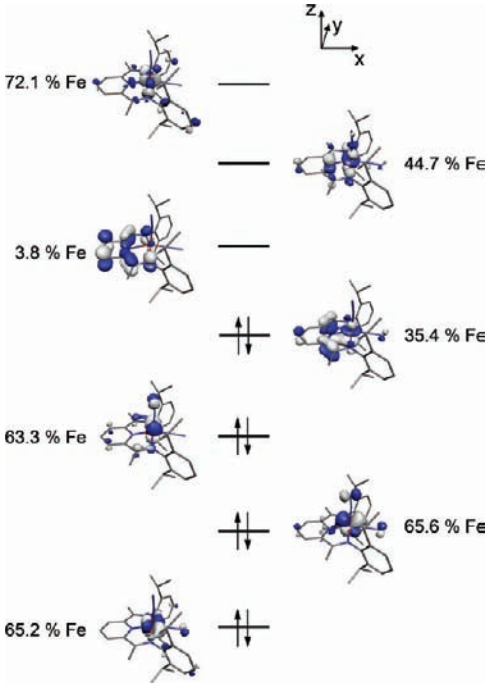

Figure 7. Qualitative MO diagram of (^{iPr}PDI)Fe(N_2)$_2$ obtained from a restricted DFT calculation at the B3LYP level.

The four-coordinate complex (^{iPr}PDI)FeN_2 was initially investigated using the same computational approaches. In contrast to the five-coordinate species, the two broken-symmetry models converged to an identical BS(2,2) solution, which is 17.1 kcal/mol more stable than the closed-shell RKS state. Furthermore, the calculated Mössbauer parameters for the broken-symmetry state (δ = 0.43 mm/s, ΔE_Q = −1.78 mm/s) are in excellent agreement with the experimental values (δ = 0.38 mm/s, ΔE_Q = 1.72 mm/s). It is important to note that the calculations yield an asymmetry parameter of the electric field gradient, η, of 0.97, which renders the sign of the computed quadrupole splitting meaningless. In contrast, the parameters for the closed-shell solution (δ = 0.40 mm/s, ΔE_Q = −0.93 mm/s) show a significant deviation in the quadrupole splitting, indicating that this state does not accurately describe the electronic structure of the compound. This is further corroborated by the optimized structures obtained by the two approaches. While both models reproduce the bond distances in the molecule, albeit with higher accuracy in the broken-symmetry case, the closed-shell solution shows a significant bend in the N_{py}−Fe−N_{N2} angle (155.79°), which is less pronounced in the broken-symmetry state and the experimental data. Therefore, the electronic structure of (^{iPr}PDI)FeN_2 is best described as (^{iPr}PDI^{2-})Fe$^{II}N_2$ with an intermediate-spin ferrous ion (S = 1) and a triplet PDI^{2-} dianion (S = 1).

At first glance, this electronic structure description of (^{iPr}PDI)FeN_2 seems to be almost identical to other square-planar PDI iron complexes with neutral ligands such as (^{iPr}PDI)Fe(DMAP). However, a closer inspection of the orbital manifold reveals important differences (Figure 8). Because of a

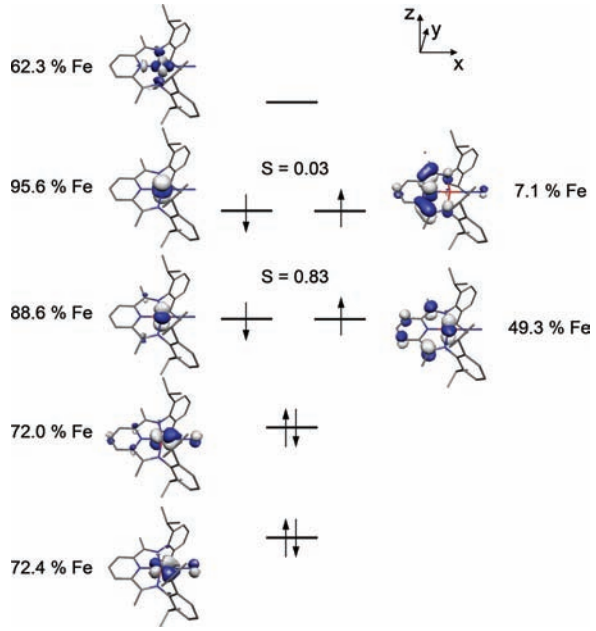

Figure 8. Qualitative MO diagram of (^{iPr}PDI)FeN_2 obtained from a BS(2,2) DFT calculation at the B3LYP level.

stabilizing interaction with the π* orbital of the dinitrogen ligand, the d_{xz} orbital is lowered in energy and doubly occupied. In exchange, the d_{z^2} orbital is now one of the two singly occupied molecular orbitals (SOMOs) on iron. This orbital has the incorrect symmetry to interact with the singly occupied ligand orbitals, which leads to a very low spatial overlap in one pair of magnetic orbitals. This is in good agreement with the population of a paramagnetic excited state at elevated temperatures for this species and prompted the investigation of higher spin states for this molecule.

A low-lying triplet state was identified using a simple unrestricted calculation. This electronic configuration was found to be only 1.1 kcal/mol higher in energy than the BS(2,2) ground state and corresponds to a (^{iPr}PDI^{-})Fe$^{I}N_2$

dx.doi.org/10.1021/ic202750n | Inorg. Chem. 2012, 51, 3770−3785

description with a low-spin Fe^{I} ion (S = 1/2) and a PDI^{-} radical (S = 1/2) with parallel spin alignment. Using the broken-symmetry formalism, a second triplet state was identified, which is 6.2 kcal/mol higher in energy than the diamagnetic ground state. In this configuration, the iron is in a high-spin Fe^{I} state (S = 3/2) that is antiferromagnetically coupled to a PDI^{-} radical (S = 1/2). The presence of these two low-lying triplet states is in good agreement with the temperature dependent magnetic behavior of (^{iPr}PDI)Fe(N_2). Thus it is likely that the d-orbital energetics and ultimately the composition of the magnetic orbitals determine whether a specific compound exhibits temperature independent paramagnetism or thermally populates a triplet excited state.

DFT studies were also conducted to further understand the XAS and XES spectroscopic data. In the case of XES a simple ground state DFT approach as previously described was employed, while for XAS full TD-DFT calculations were carried out.[67] Such approaches have been shown to be effective in both coordination compounds and metalloenzymes (and their model compounds).[56,67] Although spectroscopic transitions occur between states, simple models based on molecular orbital (MO) theory have had success in describing experimentally observed features. In this work, MO and DFT theories are additionally tested because of the presence of a redox-active ligand. All spectroscopic calculations were performed using a BP86 single-point calculation on the geometry optimized coordinates.[68−70] BP86 has been demonstrated to have a smaller error in the calculation of XAS spectra than B3LYP[71] and also improves computational efficiency. The BP86 solution was compared to the B3LYP geometry optimized electronic structure to ensure that the overall electronic structure description did not change between the two functionals. In all cases, the BP86 solution appeared more covalent, but when a broken symmetry solution existed in the B3LYP geometry optimized structure, it was reproduced when using BP86, albeit with a slightly higher overlap integral.

The TD-DFT computed XAS spectra are in good agreement with the experimental data (Figure 9). The orbitals contributing to these features were examined to determine their origins in a simple MO picture. The calculated total pre-edge intensities match experimental data well, and follow a linear trend with an R^2 = 0.85 (see Supporting Information, Figures S14−19, Table S4). The calculated pre-edge positions match the experimentally observed decrease in energy in going from five-coordinate to four-coordinate compounds. This is also predicted in a ligand-field theory model and is attributed to a decrease in the overall d-manifold energy upon decreasing coordination number.

In (^{iPr}PDI)$FeCl_2$ the calculated pre-edge is predominately due to transitions to d_{xz} (7112.1 eV) and d_{yz} (7112.4 eV) orbitals, with contributions from Cl π^* (7113.0 eV) orbitals. PDI aryl π^* and backbone π^* transitions are calculated at 7114.3 and 7115.2 eV, respectively, but with minimal intensity contributions. The pre-edges of (^{iPr}PDI)Fe$(CO)_2$ and (^{iPr}PDI)-Fe$(N_2)_2$ both derive from transitions to d_{z^2} and $d_{x^2-y^2}$ orbitals with contributions from PDI b_1 backbone π^* orbitals. Included in the calculated envelope are transitions to CO or N_2 π^* orbitals with mixing into d_{xy} and d_{xz} orbitals at 7113.2 and 7112.7 eV, respectively. These transitions appear to be experimentally resolved, corresponding to the features at 7114.5 and 7114.0 eV, respectively. The calculated shift to lower energy for the metal to ligand charge transfer (MLCT) has been previously observed and is strongly correlated to the

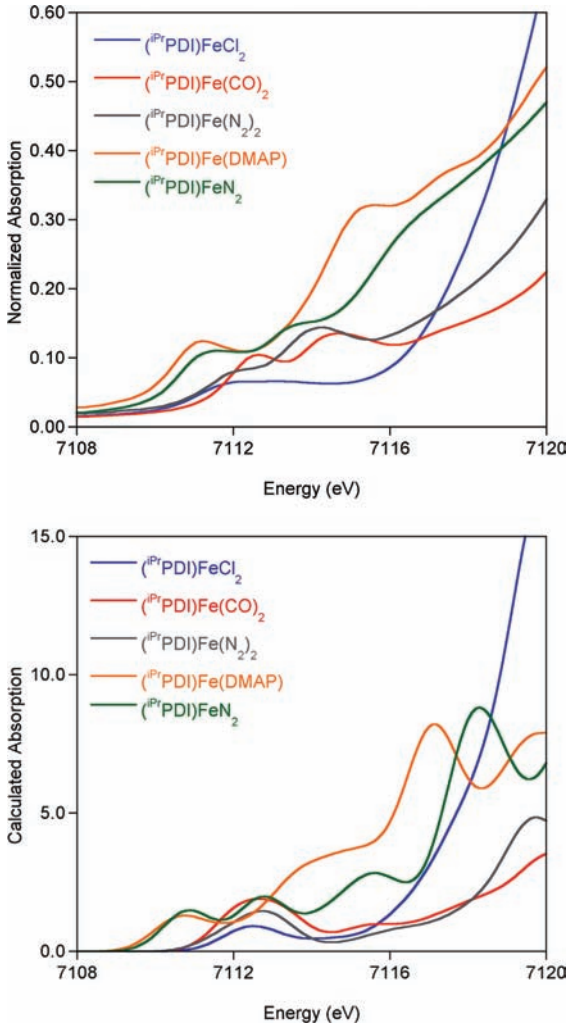

Figure 9. Experimental (top) and calculated (bottom) XAS spectra of [(^{iPr}PDI)Fe] compounds using TD-DFT. A shift of 181.25 eV and broadening of 1.5 eV have been applied to the computed spectra.

functional that is employed and in particular, the amount of Hartree−Fock mixing.[52] The first two calculated transitions are in agreement with the empty valence orbitals in the MO diagrams based on the geometry optimizations. (^{iPr}PDI)Fe-(DMAP) and (^{iPr}PDI)FeN_2, on the other hand, both have pre-edges resulting from transitions to d_{xz} orbitals with contributions from ^{iPr}PDI b_1 backbone π^* orbitals. For (^{iPr}PDI)Fe(DMAP) the calculated envelope includes a transition to a DMAP π^* orbital, and the next computationally resolved feature results from metal 4p transitions. This is in agreement with experimental spectra in which there is only one resolved feature below 7115 eV. (^{iPr}PDI)FeN_2 has a second feature at 7114.1 eV, which is computationally at 7113.4 eV, and corresponds to transitions to N_2 π^* and PDI aryl π^* orbitals. The decreasing energy shift of this transition is experimentally and computationally observed, and follows a trend in decreasing ligand field strength when going from two CO ligands (7114.5 eV exp., 7113.2 eV calc.) to two N_2 ligands (7114.1 eV exp., 7112.7 eV calc.) to one N_2 ligand (7113.4 eV exp., 7112.7 eV calc.). In all cases, the features to higher energies (above 7115.5 eV) result from transitions with contributions from both metal 4p and ligand π^* orbitals. Although TD-DFT further calculates these features to higher

dx.doi.org/10.1021/ic202750n | Inorg. Chem. 2012, 51, 3770−3785

energies, the calculations should be treated with caution, as in principle, the DFT potentials have the wrong asymptotic behavior for modeling the rising edge. Because the experimental rising edge features are well reproduced in the TD-DFT calculated spectra, they are likely not due to "shakedown" (1s to 4p plus ligand to metal charge transfer) or other multistate processes. Instead, these transitions are attributed to metal to ligand π^* or low-lying 4p transitions.

For XES calculations, studies on model compounds have demonstrated the efficacy of correlating experimental XES V2C data with a simple one-electron approximation to better understand metal–ligand bonding interactions.[54,55] This method was applied to determine whether such a model would also be also useful in systems complicated by the presence of redox active ligands. The spectra were calculated from the same BP86 solution as was used in the calculation of XAS spectra. In all cases, the calculated spectra match experimental ones quite well, both in terms of relative intensities and positions (Figure 10). The shift to higher energy of the main V2C feature for (^{iPr}PDI)FeCl$_2$ is well reproduced in the calculated spectrum (7109.1 eV), as are the relative intensities of the features at 7101.3 and 7101.4 eV for (^{iPr}PDI)FeN$_2$ and (^{iPr}PDI)Fe(N$_2$)$_2$, respectively (see Supporting Information for table). In both the experimental and calculated spectra, the intensity of this feature is greater for (^{iPr}PDI)Fe(N$_2$)$_2$ than (^{iPr}PDI)FeN$_2$ (relative to the other V2C features).

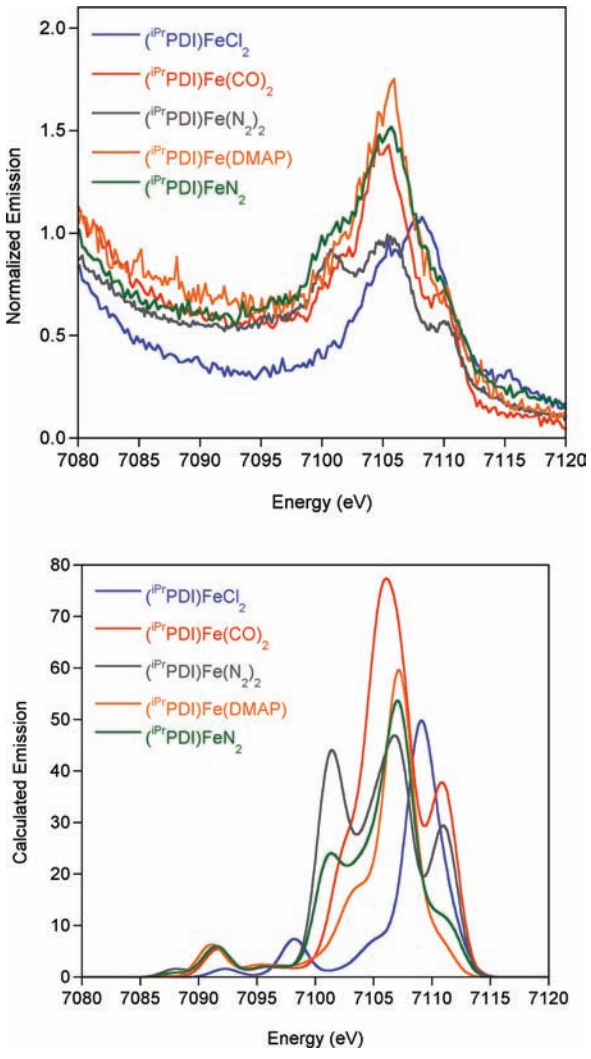

Figure 10. Experimental (top) and calculated (bottom) V2C spectra for the [(^{iPr}PDI)Fe] compounds. A broadening of 2.5 eV and a shift of 182.5 eV have been applied to the computed spectra.

The calculated spectra were further examined to determine the origin of each transition. Most notable is the feature between 7101 and 7104 eV, which corresponds to a non-PDI ligand (N$_2$, DMAP or CO) 2p or (Cl) 3p to metal 1s transition. In both the experimental and computed spectra it is approximately twice as intense for (^{iPr}PDI)Fe(N$_2$)$_2$ as for (^{iPr}PDI)FeN$_2$ (Figures 11, 12), suggesting that this feature is sensitive to N$_2$ coordination number. Deconvolutions of the calculated spectra using MO Analyzer[72] to separate ligand versus metal contributions demonstrate that this feature is predominantly due to transitions from non-PDI ligand orbitals (Figure 13). (^{iPr}PDI)FeCl$_2$ has the weakest spectral contributions from the PDI ligand, which could either reflect the high spin state at iron (and thus a small amount of iron p mixing), or the PDI^0 oxidation state. To highest energies (peaks g or h), the feature is experimentally and computationally more intense for (^{iPr}PDI)Fe(CO)$_2$ and (^{iPr}PDI)Fe(N$_2$)$_2$ and corresponds to a ligand orbital with metal d_{z^2} contributions. For (^{iPr}PDI)Fe(DMAP) and (^{iPr}PDI)FeN$_2$, this feature results from a ligand orbital with some metal mixing, and is much less intense. For all compounds, the orbital contributing to the intensity of the highest feature in calculated XES is an orbital of the same symmetry and similar composition to the orbital that contributes to the first pre-edge transition in the calculated XAS spectra. Studies are underway in our laboratory to further understand the observed XES transitions from occupied α spin orbitals and XAS transitions to unoccupied β spin orbitals of similar compositions.

CONCLUDING REMARKS

The electronic structures of the four- and five-coordinate bis(imino)pyridine iron dinitrogen complexes, (^{iPr}PDI)FeN$_2$ and (^{iPr}PDI)Fe(N$_2$)$_2$, have been established by a combination of spectroscopic and computational methods. The four-coordinate compound is best described as an intermediate spin iron(II) derivative antiferromagnetically coupled to a bis(imino)pyridine diradical dianion. The SOMOs of the iron are principally d_{yz} and d_{z^2}, the latter of the two has the incorrect symmetry to effectively couple with the orbitals of the bis(imino)pyridine. This ground state description is similar to (^{iPr}PDI)Fe(DMAP) and other four-coordinate bis(imino)-pyridine iron compounds with primarily σ-donating ligands. These compounds are also best described as intermediate spin ferrous compounds with triplet bis(imino)pyridine diradical dianions. However, in these cases, the SOMOs are composed of two cloverleaf d-orbitals of the appropriate symmetry to strongly couple to the chelate diradical. As a consequence, the NMR spectroscopic behavior of (^{iPr}PDI)FeN$_2$ and the (^{iPr}PDI)Fe(DMAP) is dramatically different. The weak coupling in the former compound gives rise to temperature dependent chemical shifts arising from thermal population of a triplet excited state. By contrast, the strong coupling in the (^{iPr}PDI)Fe(DMAP) class of compounds exhibit temperature independent paramagnetism arising from mixing of a triplet excited state into the ground state by spin orbit coupling. The five-coordinate bis(imino)pyridine iron bis(dinitrogen) compound, (^{iPr}PDI)Fe(N$_2$)$_2$, differs from the four-coordinate species and is best described as a highly covalent compound

dx.doi.org/10.1021/ic202750n | Inorg. Chem. 2012, 51, 3770–3785

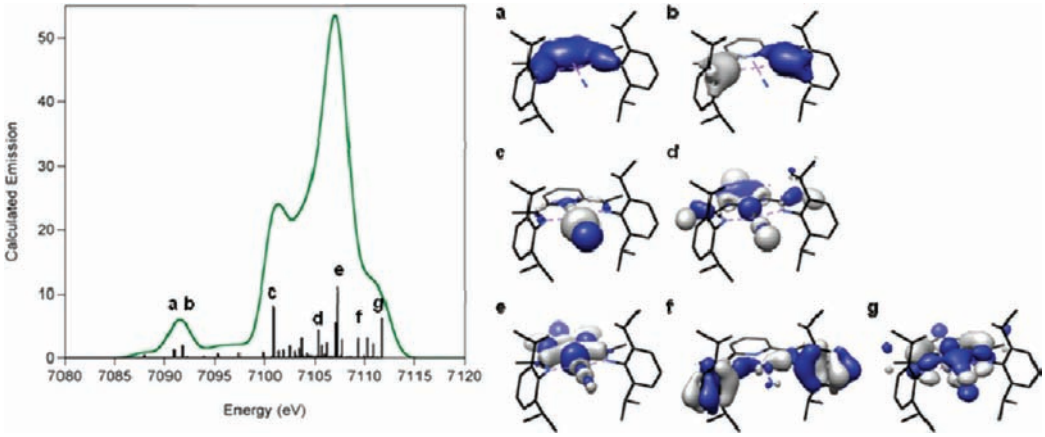

Figure 11. Calculated V2C spectrum of (^{iPr}PDI)FeN$_2$ with the molecular orbitals that strongly contribute to the observed transitions. A broadening of 2.5 eV and a shift of 182.5 eV have been applied.

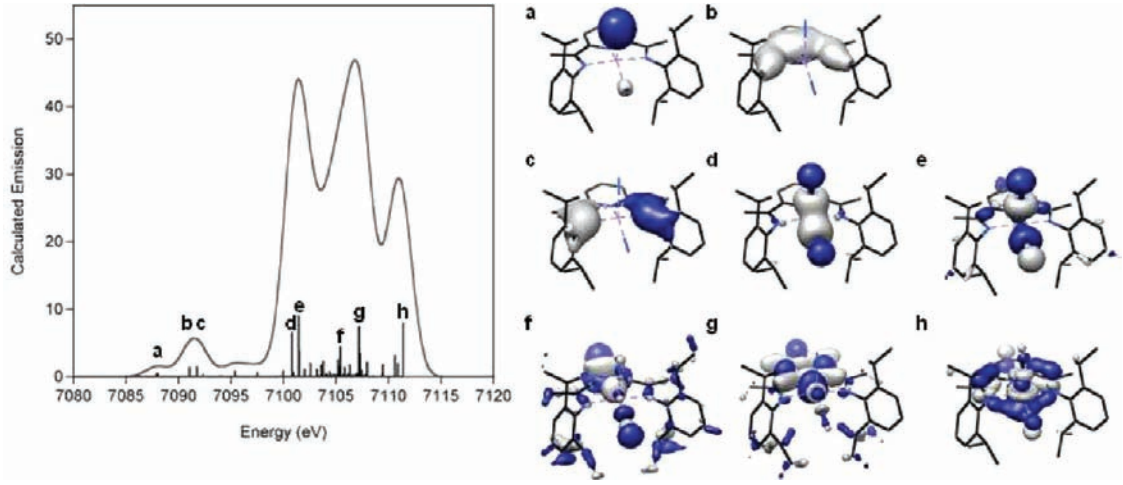

Figure 12. Calculated V2C spectrum of (^{iPr}PDI)Fe(N$_2$)$_2$ with the molecular orbitals that strongly contribute to the observed transitions. A broadening of 2.5 eV and a shift of 182.5 eV have been applied.

that is a hybrid between Fe(0) and low spin Fe(II) canonical forms supporting the originally proposed electronic structure description for this compound. The high covalency of this electronic structure regime is also observed in dimeric, five-coordinate iron dinitrogen compounds. Thus, dissociation of a dinitrogen ligand results in a measurable difference in ligand field such that a spin state change occurs at iron from low to intermediate spin. Accordingly, the redox-active and non-innocent bis(imino)pyridine ligand is electronically flexible and shifts its electronic structure to meet the requirements of the metal.

EXPERIMENTAL SECTION

General Considerations. All air- and moisture-sensitive manipulations were carried out using standard vacuum line, Schlenk, and cannula techniques or in an MBraun inert atmosphere drybox containing an atmosphere of purified nitrogen. Solvents for air- and moisture-sensitive manipulations were initially dried and deoxygenated using literature procedures.[73] Benzene-d_6 was purchased from Cambridge Isotope Laboratories and dried over 4 Å molecular sieves. (^{iPr}PDI)Fe(CO)$_2$,[17] (^{iPr}PDI)Fe(DMAP)[19] were synthesized according to literature procedures. (^{iPr}PDI)Fe(N$_2$)$_2$, was synthesized using the published method 2.[17] (^{iPr}PDI)FeN$_2$ was synthesized according to the published method 1.[17]

^{1}H NMR spectra were recorded on Inova-400 and -500 spectrometers (operating at 400 and 500 mHz, respectively) equipped with a 5 mm QuadraProbe (^{1}H/^{19}F/^{31}P/^{13}C) and 5 mm ^{1}H/BB (^{15}N−^{31}P) tunable probe, respectively. All ^{1}H NMR shifts are reported relative to SiMe$_4$, using ^{1}H (residual) chemical shifts of the solvent as a secondary standard. Elemental analyses were performed at Robertson Microlit Laboratories, Inc., Ledgewood, NJ.

Solution magnetic moments were determined by the method of Evans[74] using a ferrocene standard and are the average value of two to three independent measurements. Solid state magnetic susceptibility measurements were performed with a Johnson Mathey magnetic susceptibility balance (MSB) that was calibrated with HgCo(SCN)$_4$ or using SQUID magnetrometry.

X-ray Absorption Spectroscopy. Samples were prepared in an inert atmosphere nitrogen glovebox as finely ground dilutions in boron nitride pressed into 1 mm Al spacers and shipped to the experimental site in triple glass jars with fluoropolymer seals on the lids and sealed with Teflon and electrical tape. Spacers for (^{iPr}PDI)Fe(N$_2$)$_2$ were prepared in a glovebox and immediately transferred to a plastic vial in liquid nitrogen and shipped at cryogenic temperature to the experimental site. Following the experiment, the sample was checked for decay to the four-coordinate compound, (^{iPr}PDI)FeN$_2$, by solid state IR spectroscopy in KBr. X-ray absorption spectra were recorded at the Stanford Synchrotron Radiation Lightsource (SSRL) on beamlines BL9-3 ((^{iPr}PDI)FeCl$_2$) and BL7-3 (all other compounds) under standard ring conditions. The beamline optics were optimized, and the monochromator was fully tuned at 7500 eV. The incident energy was calibrated by setting the first inflection of an iron foil to 7111.2 eV. Data were measured in transmission mode.

dx.doi.org/10.1021/ic202750n | Inorg. Chem. 2012, 51, 3770−3785

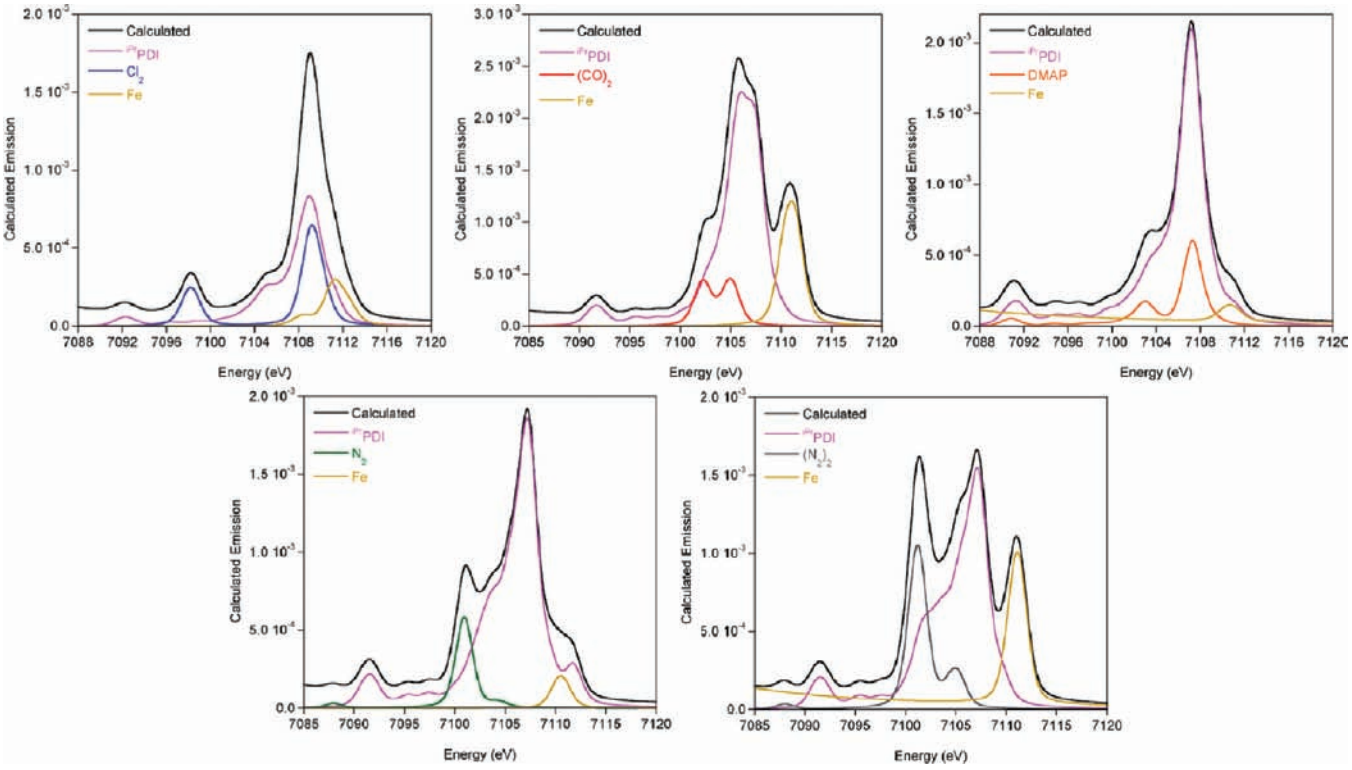

Figure 13. Calculated XES spectra of (^{iPr}PDI)Fe compounds showing deconvolutions based on ligand identity and metal contributions. A threshold of 40% was used in assigning ligand contributions, and a threshold of 25% was used for metal d contributions. A shift of 182.5 eV has been applied.

The fitting program EDG_FIT[53] was used to quantify pre-edge areas using linear least-squares fits. The pre-edge features were modeled with line shapes having fixed mixings of a 50:50 ratio of Lorentzian and Gaussian functions (pseudo-Voigt). The background was modeled with both a fixed pseudo-Voigt function, as well as with a function where the mixing was floated to allow a closer fit. Both of these possibilities were fit over several energy ranges: 7108−7116, 7108−7118, 7108−7120, and 7108−7125 eV. The fit and the second derivative of the fit were compared to the data to determine the quality of a given fit. The areas of the fits were determined using two different methods. The first method, which was previously published (and is referred to as the triangle method), approximates the area by height times the full width at half-maximum (fwhm).[45] The second method uses Simpson's Rule, as previously reported, to integrate the area.[56]

X-ray Emission Spectroscopy. All samples were prepared in the same manner as for XAS experiments. XES data for (^{iPr}PDI)FeCl$_2$, (^{iPr}PDI)Fe(CO)$_2$, (^{iPr}PDI)FeN$_2$, and (^{iPr}EtPDI)FeN$_2$ were measured at the C-Line at the Cornell High Energy Synchrotron Source (CHESS), and data for (^{iPr}PDI)Fe(N$_2$)$_2$ and (^{iPr}PDI)Fe(DMAP) were collected at beamline 6-2 at Stanford Synchrotron Radiation Lightsource (SSRL). The incident energy was set to 9 keV utilizing either a Si(111) monochromator (∼ 1 eV bandwidth, SSRL) or multilayers (∼90 eV bandwidth, CHESS). The energy of the incident beam was calibrated with either an iron foil (SSRL), setting the first inflection point to 7111.2 eV, or a Ni or Cu foil (CHESS), setting the first inflection point to 8330 and 8979 eV, respectively.

XES spectra were recorded with a crystal array spectrometer, which employs three spherically bent Ge(620) crystals (100 mm diameter, 1 m radius of curvature) aligned on intersecting Rowland circles.[58] A silicon drift detector was used to detect the resultant fluoresecence. Samples were positioned at 45 degrees with respect to the incident beam, and were maintained at a temperature of less than 100 K with an ARS helium displex cryostat (CHESS) or Oxford CF1208 cryostat (SSRL). A helium-filled flight path was utilized between the cryostat and the spectrometer to minimize signal attenuation of the fluorescence.

Iron Kβ XES spectra were collected from 7030 to 7120 eV with a step size of +0.2 eV over the K$\beta_{1,3}$ line (7020−7070 eV) and a step size of +0.15 eV over the K$\beta_{2,5}$ line (7070−7120 eV). Spectra were normalized to the incident flux I_0 measured in a He-filled ion chamber (SSRL) or N_2-filled (CHESS). The spectrometer energy resolution is estimated at ∼2.5 eV. Fe_2O_3 was used as a reference sample to calibrate the spectrometer energy between different experimental runs, with the maximum of the K$\beta_{1,3}$ line calibrated to 7060.6 eV and the maximum of the K$\beta_{2,5}$ line calibrated to 7107.2 eV. The resulting calibration error in this study was 0.3 eV between those samples measured at CHESS versus those measured at SSRL.

For all samples, damage scans were performed to estimate the stability of the samples with respect to radiation. The averaged data represent only those scans, which showed no evidence of radiation damage. The data were processed and averaged using the programs PyMca (CHESS), and the SamView component of SixPACK (SSRL).[75,76] The data were normalized and fit using the program BlueprintXAS.

Quantum Chemical Calculations. All DFT calculations were performed with the ORCA program package.[77] The geometry optimizations of the complexes and single-point calculations on the optimized geometries were carried out at the B3LYP level[69,70,78] of DFT. This hybrid functional often gives better results for transition metal compounds than pure gradient-corrected functionals, especially with regard to metal−ligand covalency.[79] The all-electron Gaussian basis sets were those developed by the Ahlrichs group.[80−82] Triple-ζ quality basis sets def2-TZVP with one set of polarization functions on the metals and on the atoms directly coordinated to the metal center were used. For the carbon and hydrogen atoms, slightly smaller polarized split-valence def2-SV(P) basis sets were used, that were of double-ζ quality in the valence region and contained a polarizing set of d-functions on the non-hydrogen atoms. Auxiliary basis sets were chosen to match the orbital basis.[83−85] The RIJCOSX[86−88] approximation was used to accelerate the calculations.

Throughout this paper we describe our computational results by using the broken-symmetry (BS) approach by Ginsberg[89] and Noodleman et al.[90] Because several broken symmetry solutions to

dx.doi.org/10.1021/ic202750n | Inorg. Chem. 2012, 51, 3770−3785

the spin-unrestricted Kohn–Sham equations may be obtained, the general notation BS(m,n)[91] has been adopted, where m (n) denotes the number of spin-up (spin-down) electrons at the two interacting fragments. Canonical and corresponding[92] orbitals, as well as spin density plots were generated with the program Molekel.[93]

Nonrelativistic single-point calculations on the optimized geometry were carried out to predict Mössbauer spectral parameters (isomer shifts and quadrupole splittings). These calculations employed the CP(PPP) basis set for iron.[94] The Mössbauer isomer shifts were calculated from the computed electron densities at the iron centers as previously described.[66,95]

Spectroscopic Calculations. Single-point spectroscopic calculations were done on the geometry optimized structures and used the BP86 functional along with the TZVP basis set for all carbon, nitrogen, and hydrogen atoms, and the expanded basis, CP(PPP),[91] for iron. CP(PPP) utilizes Core-prop which is based on the TurboMole DZ basis developed by the Ahlrichs group,[96] as well as polarization functions developed by the same group.[97] The conductor-like infinite dielectric screening model, COSMO, was used (ε = 9.08).[98] A dense integration grid (grid4 nofinalgrid) was used, with a special grid integration accuracy of 7 specified for iron to increase the radial integration accuracy. These single-point calculations were qualitatively examined to confirm that the general electronic structure description remained the same. The Mössbauer shifts were calculated as previously described.[66,95]

TD-DFT was used to predict transitions to the pre-edge region of the Fe K-edge XAS spectra with invoked quadrupole and magnetic dipole transitions.[67] Symmetry equivalent 1s orbitals were localized using the Pipek-Mezey criteria,[99] and only singlet excitations from localized iron 1s orbitals were allowed. The maximum number of expansion vectors allowed in the iterative solution were 450, and 400 roots were used. The calculated energies were shifted according to calibration studies on known ferrous and ferric complexes using the computational parameters as described in this work, and following previously published calibration methods.[56] Calculated XAS spectra (ABSQ) were plotted using ORCA_MAPSPC over a range of 6500–7500 eV with a weighting of 1.5 eV, and 10,000 points. Only transitions that contained iron d character (as determined by the Löwdin populations) were included for the calculated pre-edge positions and areas. The experimental pre-edge areas were compared to the sum of the transition intensities (with an intensity weighted average for position) and the average of the full oscillator strengths for all transitions to d orbitals.

The XES spectra were calculated using the simple one-electron approximation as previously described.[54] Calculated XES spectra (XESQ) were plotted using ORCA_MAPSPC over a range of 6000–7000 eV with a weighting of 2.5 eV, and 10,000 points. All orbitals and spin density distributions were plotted using Chimera.[100] XAS and XES spectra were visualized using Kaleidagraph.[101] XES deconvolutions were visualized using MOanalyzer.[72,102]

Preparation of (^{iPr}EtPDI)FeN$_2$. A 100 mL round-bottom flask was charged with 0.054 g (2.36 mmol) of sodium metal and approximately 20 mL of toluene. With stirring, 10.80 g (53.84 mmol) of mercury was added to the flask followed by 0.300 g (0.471 mmol) of (^{iPr}EtPDI)FeCl$_2$. The reaction mixture was stirred for 15 min after which time the resulting dark green solution was filtered through Celite, and the toluene removed in vacuo. The solid was washed with 3 × 0.5 mL of pentane, and the resulting solid was dried for approximately one minute to prevent dinitrogen loss. This procedure yielded 0.187 g (67%) of a dark green solid identified as (^{iPr}EtPDI)FeN$_2$. Analysis for $C_{35}H_{47}N_5Fe$: Calc. C, 70.81; H, 7.98; N, 11.80. Found: C, 71.12; H, 7.80; N, 11.55. ^{1}H NMR (benzene-d$_6$, 20 °C): δ = −0.78 (d, 12H, CH-(CH_3)$_2$), 1.24 (m, 4H, CH-(CH$_3$)$_2$), 1.32 (d, 12H, CH-(CH_3)$_2$), 2.06 (t, 6H, CH$_2$CH_3), 2.64 (t, 1H, *p-py*), 7.69 (m, 6H, *m* and *p-Ar*), 8.78 (q, 4H, CH_2CH$_3$), 10.33(d, 2H, *m-py*). ^{13}C{^{1}H} NMR (benzene-d$_6$): δ = 5.0 (CH$_2$CH$_3$), 24.5 (Ar-CH(CH$_3$)$_2$), 34.2 (Ar–CH(CH$_3$)$_2$), 36.9 (CH(CH$_3$)$_2$), 61.0 (CH$_2$CH$_3$), 77.4 (*m*-pyr), 125.3 (*aryl*), 126.8 (*aryl*), 128.4 (*aryl*), 141.8 (*aryl*), 145.9 (*aryl*), 154.5 (*aryl*), 167.5 (*aryl*), 213.3 (*p*-pyr). IR(pentane): ν(N$_2$) = 2045 cm^{-1}. IR(KBr): ν(N$_2$) = 2027 cm^{-1}.

Preparation of (^{iPr}iPrPDI)FeN$_2$. This molecule was prepared in a manner similar to (^{iPr}EtPDI)FeN$_2$ using 0.034 g (1.50 mmol) of sodium metal, 6.919 g (34.49 mmol) of mercury, and 0.200 g (0.300 mmol) of (^{iPr}iPrPDI)FeCl$_2$. Recrystallization from pentane at −35 °C furnished 0.104 g (56%) of a dark green solid identified as (^{iPr}iPrPDI)FeN$_2$. Analysis for $C_{37}H_{51}N_5Fe$: Calc. C, 71.48; H, 8.27; N, 11.27. Found: C, 71.72; H, 8.05; N, 11.06. ^{1}H NMR (benzene-d$_6$, 20 °C): δ = −1.37 (d, 12H, CH-(CH_3)$_2$), −1.26 (t, 1H, *p-py*), 1.28 (m, 4H, CH-(CH$_3$)$_2$), 1.40 (d, 12H, CH-(CH_3)$_2$), 3.69 (d, 12H, CH-(CH_3)$_2$), 4.36 (m, 2H, CH-(CH$_3$)$_2$), 7.82 (t, 2H, *p-Ar*), 7.93 (d, 4H, *m-Ar*), 11.69 (d, 2H, *m-py*). ^{13}C{^{1}H} NMR (benzene-d$_6$): δ = −3.5 (CH(CH$_3$)$_2$), 25.2 (Ar-CH(CH$_3$)$_2$), 38.5 (Ar–CH(CH$_3$)$_2$), 42.1 (CH(CH$_3$)$_2$), 55.0 (CH(CH$_3$)$_2$), 88.0 (*m*-pyr), 124.4 (*aryl*), 129.2 (*aryl*), 133.3 (*aryl*), 134.6 (*aryl*), 165.8 (*aryl*), 193.2 (*p*-pyr). IR(pentane): ν(N$_2$) = 2044 cm^{-1}. IR(KBr): ν(N$_2$) = 2026 cm^{-1}.

■ ASSOCIATED CONTENT

Supporting Information

X-ray crystallographic data for (^{iPr}EtPDI)FeN$_2$ and (^{iPr}iPr PDI)FeN$_2$ in cif format. SQUID, Mössbauer, IR, VT-XAS, XES fits, and calculated XAS and XES deconvolutions. This material is available free of charge via the Internet at http://pubs.acs.org.

■ AUTHOR INFORMATION

Corresponding Author

*E-mail: pchirik@princeton.edu (P.J.C.).

Notes

The authors declare no competing financial interest.

■ ACKNOWLEDGMENTS

P.J.C. and K.W. thank the U.S. National Science Foundation and Deutsche Forschungsgemeinschaft for a Cooperative Activities in Chemistry between U.S. and German Investigators grant. S.D. acknowledges the Department of Chemistry and Chemical Biology at Cornell University, the Max Planck Society, the Sloan Foundation, and an ACS Petroleum Research Fund Grant (50270-DN13) for generous financial support. S.C.E.S. thanks NSF for a graduate research fellowship (DGE-0646086) for support. C.M. is grateful to the Alexander von Humboldt Foundation for a postdoctoral research fellowship. This work is based, in part, upon research conducted at the Cornell High Energy Synchrotron Source (CHESS), which is supported by the National Science Foundation and the National Institutes of Health/National Institute of General Medical Sciences under NSF award DMR-0936384. Portions of the research were carried out at the Stanford Synchrotron Radiation Lightsource, a national user facility operated by Stanford University on behalf of the DOE, BES. The SSRL SMB Program is supported by DOE, BER and NIH, NCRR, BMTP. Some of the simulations presented in this article were performed on computational resources supported by the Princeton Institute for Computational Science and Engineering (PICSciE) and the Office of Information Technology's High Performance Computing Center and Visualization Laboratory at Princeton University. We also thank Suzanne Bart and Amanda Bowman for experimental assistance.

■ REFERENCES

(1) Hazari, N. *Chem. Soc. Rev.* **2010**, *39*, 4044.
(2) Sacco, A.; Aresta, M. *Chem. Commun.* **1968**, 1223.
(3) Borodko, Y. G.; Broitman, M. O.; Kachapina, L. M.; Shilov, A. E.; Ukhin, L. Y. *J. Chem. Soc. D* **1971**, 1185.
(4) Schrauzer, G. N.; Guth, T. D. *J. Am. Chem. Soc.* **1976**, *98*, 3508.

(5) Leigh, G. J.; Jiminez-Tenorio, M. *J. Am. Chem. Soc.* **1991**, *113*, 5862.
(6) (a) Chatt, J. *Philos. Trans. R. Soc., B* **1977**, *281*, 243. (b) Chatt, J.; Pearman, A. J.; Richards, R. J. *J. Chem. Soc., Dalton Trans.* **1977**, 1852.
(7) (a) Smith, J. M.; Lachicotte, R. J.; Pittard, K. A.; Cundari, T. R.; Lukat-Rodgers, G.; Rodgers, K. R.; Holland, P. L. *J. Am. Chem. Soc.* **2001**, *123*, 9222. (b) Smith, J. M.; Sadique, A. R.; Cundari, T. R.; Rodgers, K. R.; Lukat-Rodgers, G.; Lachicotte, R. H.; Flaschenriem, C. J.; Vela, J.; Holland, P. L. *J. Am. Chem. Soc.* **2006**, *128*, 756.
(8) (a) Gilbertson, J. D.; Szymczak, N. K.; Tyler, D. R. *J. Am. Chem. Soc.* **2005**, *127*, 10184. (b) Yelle, R. B.; Crossland, J. L.; Szmczak, N. K.; Tyler, D. R. *Inorg. Chem.* **2009**, *48*, 861. (c) Crossland, J. L.; Balesdent, C. G.; Tyler, D. R. *Dalton Trans.* **2009**, 4420.
(9) Rodriguez, M. M.; Bill, E.; Brennessel, W. W.; Holland, P. L. *Science* **2011**, *11*, 780.
(10) (a) Saouma, C. T.; Peters, J. C. *Coord. Chem. Rev.* **2011**, *255*, 920. (b) Saouma, C. T.; Kinney, R. A.; Hoffmann, B. M.; Peters, J. C. *Angew. Chem., Int. Ed.* **2011**, *50*, 3446. (c) Takaoka, A.; Mankad, N. P.; Peters, J. C. *J. Am. Chem. Soc.* **2011**, *133*, 8440. (d) Saouma, C. T.; Müller, P.; Peters, J. C. *J. Am. Chem. Soc.* **2009**, *131*, 10358. (e) Whited, M. T.; Mankad, N. P.; Lee, Y.; Oblad, P. F.; Peters, J. C. *Inorg. Chem.* **2009**, *48*, 2507. (f) Crossland, J. L.; Zakharov, L. N.; Tyler, D. R. *Inorg. Chem.* **2007**, *46*, 10476. (g) Hendrich, M. P.; Gunderson, W.; Behran, R. K.; Green, M. T.; Mehn, M. P.; Betley, T. A.; Lu, C. C.; Peters, J. C. *Proc. Natl. Acad. Sci. U.S.A.* **2006**, *103*, 17107.
(11) Betley, T. A.; Peters, J. C. *J. Am. Chem. Soc.* **2003**, *125*, 10782.
(12) Moret, M.-E.; Peters, J. C. *J. Am. Chem. Soc.* **2011**, *133*, 18118.
(13) (a) Whetten, R. L.; Fu, K.-J.; Grant, E. R. *J. Am. Chem. Soc.* **1982**, *104*, 4270. (b) Weiller, B. H.; Miller, M. E.; Grant, E. R. *J. Am. Chem. Soc.* **1987**, *109*, 352. (c) Wuu, Y.-M.; Bentsen, J. G.; Brinkley, C. G.; Wrighton, M. S. *Inorg. Chem.* **1987**, *26*, 530. (d) Hayes, D.; Weitz, E. *J. Phys. Chem.* **1991**, *95*, 2723. (e) Snee, P. T.; Payne, C. K.; Mebane, S. D.; Kotz, K. T.; Harris, C. B. *J. Am. Chem. Soc.* **2001**, *123*, 6909.
(14) (a) Schroeder, M. A.; Wrighton, M. S. *J. Am. Chem. Soc.* **1976**, *98*, 551. (b) Mitchener, J. C.; Wrighton, M. S. *J. Am. Chem. Soc.* **1981**, *103*, 975.
(15) (a) Small, B. L.; Brookhart, M.; Bennett, A. M. A. *J. Am. Chem. Soc.* **1998**, *120*, 4049. (b) Britovsek, G. J. P.; Gibson, V. C.; Kimberley, B. S.; Maddox, P. J.; McTavish, S. J.; Solan, G. A.; White, A. J. P.; Williams, D. J. *Chem. Commun.* **1998**, 849. (c) Small, B. L.; Brookhart, M. *Macromolecules* **1999**, *32*, 2120.
(16) Gibson, V. C.; Redshaw, C.; Solan, G. A. *Chem. Rev.* **2007**, *107*, 1745.
(17) Bart, S. C.; Lobkovsky, E.; Chirik, P. J. *J. Am. Chem. Soc.* **2004**, *126*, 13794.
(18) Scott, J.; Vidyaratne, I.; Korobkov, I.; Gambarotta, S.; Budzelaar, P. H. M. *Inorg. Chem.* **2008**, *47*, 896.
(19) Bart, S. C.; Chlopek, K.; Bill, E.; Bouwkamp, M. W.; Lobkovsky, E.; Neese, F.; Wieghardt, K.; Chirik, P. J. *J. Am. Chem. Soc.* **2006**, *128*, 13901.
(20) Tondreau, A. M.; Milsmann, C.; Lobkovsky, E.; Chirik, P. J. *Inorg. Chem.* **2011**, *50*, 9888.
(21) Bart, S. C.; Lobkovsky, E.; Bill, E.; Weighardt, K.; Chirik, P. J. *Inorg. Chem.* **2007**, *46*, 7055.
(22) Jørgensen, C. K. *Coord. Chem. Rev.* **1966**, *1*, 164.
(23) Chirik, P. J. *Inorg. Chem.* **2011**, *50*, 9737.
(24) Knijnenburg, D.; Hetterscheid, D.; Kooistra, T. M.; Budzelaar, P. H. M. *Eur. J. Inorg. Chem.* **2004**, 1204.
(25) Kuwabara, I. H.; Comninos, F. C. M.; Pardini, V. L.; Viertler, H.; Toma, H. E. *Electrochim. Acta* **1994**, *39*, 2401.
(26) Toma, H. E.; Chavez-Gil, T. E. *Inorg. Chim. Acta* **1997**, *257*, 197.
(27) de Bruin, B.; Bill, E.; Bothe, E.; Weyermüller, T.; Wieghardt, K. *Inorg. Chem.* **2000**, *39*, 2936.
(28) Budzelaar, P. H. M.; de Bruin, B.; Gal, A. W.; Wieghardt, K.; van Lenthe, J. H. *Inorg. Chem.* **2001**, *40*, 4649.
(29) Chaudhuri, P.; Wieghardt, K. *Prog. Inorg. Chem.* **2001**, *50*, 151.
(30) Knijnenburg, Q.; Gambarotta, S.; Budzelaar, P. H. M. *Dalton Trans.* **2006**, 5442.
(31) Butin, K. P.; Beloglazkina, E. K.; Zyk, N. V. *Russ. Chem. Rev.* **2005**, *74*, 531.
(32) Bowman, A. C.; Bart, B. C.; Heinemann, F. W.; Meyer, K.; Chirik, P. J. *Inorg. Chem.* **2009**, *48*, 5587.
(33) Russell, S. K.; Darmon, J. M.; Lobkovsky, E.; Chirik, P. J. *Inorg. Chem.* **2010**, *49*, 2782.
(34) Archer, A. M.; Bouwkamp, M. W.; Cortez, M.-P.; Lobkovsky, E.; Chirik, P. J. *Organometallics* **2006**, *25*, 4269.
(35) Trovitch, R. J.; Lobkovsky, E.; Bill, E.; Chirik, P. J. *Organometallics* **2008**, *27*, 1470.
(36) Tondreau, A. M.; Atienza, C. C. H.; Weller, K. J.; Nye, S. A.; Lewis, K. M.; Delis, J. G. P.; Chirik, P. J. *Science* **2012**, *335*, 567.
(37) Bouwkamp, M. W.; Bowman, A. C.; Lobkovsky, E.; Chirik, P. J. *J. Am. Chem. Soc.* **2006**, *128*, 13340.
(38) Russell, S. K.; Lobkovsky, E.; Chirik, P. J. *J. Am. Chem. Soc.* **2011**, *133*, 8858.
(39) Sylvester, K. T.; Chirik, P. J. *J. Am. Chem. Soc.* **2009**, *131*, 8772.
(40) McTavish, S.; Britovsek, G. J. P.; Smit, T. M.; Gibson, V. C.; White, A. J. P.; Williams, D. J. *J. Mol. Catal.* **2007**, *261*, 293−300.
(41) Zhu, D.; Thapa, I.; Korobkov, I.; Gambarotta, S.; Budzelaar, P. H. M. *Inorg. Chem.* **2011**, *50*, 9879.
(42) Bowman, A. C.; Milsman, C.; Bill, E.; Lobkovsky, E.; Weyermüller, T.; Wieghardt, K.; Chirik, P. J. *Inorg. Chem.* **2010**, *49*, 6110.
(43) Shulman, G. R.; Yafet, Y.; Eisenberger, P.; Blumberg, W. E. *Proc. Natl. Acad. Sci. U.S.A.* **1976**, *73*, 1384.
(44) Levina, A.; Armstrong, R. S.; Lay, P. A. *Coord. Chem. Rev.* **2005**, *249*, 141.
(45) Westre, T. E.; Kennepohl, P.; DeWitt, J. G.; Hedman, B.; Hodgson, K. O.; Solomon, E. I. *J. Am. Chem. Soc.* **1997**, *119*, 6297.
(46) Bowman, A. C.; Milsmann, C.; Atienza, C. C. H.; Lobkovsky, E.; Wieghardt, K.; Chirik, P. J. *J. Am. Chem. Soc.* **2010**, *132*, 1676.
(47) (a) Ramallo-López, J. M.; Lede, E. J.; Requejo, F. G.; Rodriguez, J. A.; Kim, J.- Y.; Rosas-Salas, R.; Domínguez, J. M. *J. Phys. Chem. B* **2004**, *108*, 20005. (b) Honji, A.; Gron, L. U.; Chang, J.-R.; Gates, B. C. *Langmuir* **1992**, *8*, 2715.
(48) Ruiz-Lopez, M.; Loos, M.; Goulon, J.; Benfatto, M.; Natoli, C. R. *Chem. Phys.* **1988**, *121*, 419.
(49) Balasubramanian, M.; Giacomini, M. T.; Lee, H. S.; McBreen, J.; Sukamoto, J. H. *J. Electrochem. Soc.* **2002**, 149.
(50) Cartier, C.; Momenteau, M.; Dartyge, E.; Fontaine, A.; Tourillon, G.; Michalowicz, A.; Verdaguer, M. *J. Chem. Soc., Dalton Trans.* **1992**, 609.
(51) Bair, R. A.; Goddard, W. A. III *Phys. Rev. B* **1980**, *22*, 2767.
(52) Roemelt, M.; Beckwith, M. A.; Duboc, C.; Collomb, M.-N.; Neese, F.; DeBeer, S. *Inorg. Chem.* **2012**, *51* (1), 680.
(53) George, G. N. *EXAFSPAK, SSRL, SLAC*; Stanford University: Stanford, CA, 2000.
(54) Lee, N.; Petrenko, T.; Bergmann, U.; Neese, F.; DeBeer, S. *J. Am. Chem. Soc.* **2010**, *132*, 9715.
(55) (a) Lancaster, K. M.; Finkelstein, K. D.; DeBeer, S. *Inorg. Chem.* **2011**, *50*, 6767. (b) Beckwith, M. A.; Roemelt, M.; Collomb, M.; DuBoc, C.; Weng, T.; Bergmann, U.; Glatzel, P.; Neese, F.; DeBeer, S. *Inorg. Chem.* **2011**, *50*, 8397.
(56) Chandrasekaran, P.; Stieber, S. C. E.; Collins, T. J.; Que,, L.; Neese, F.; DeBeer, , S. *Dalton Trans.* **2011**, *40*, 11070.
(57) de Groot, F. *Chem. Rev.* **2001**, *101*, 1779.
(58) Glatzel, P.; Bergmann, U. *Coord. Chem. Rev.* **2005**, *249*, 65.
(59) Bergmann, U.; Horne, C. R.; Collins, T. J.; Workman, J. M.; Cramer, S. P. *Chem. Phys. Lett.* **1999**, *302*, 119.
(60) Bergmann, U.; Bendix, J.; Glatzel, P.; Gray, H. B.; Cramer, S. P. *J. Chem. Phys.* **2002**, *116*, 2011.
(61) Vankó, G.; Neisius, T.; Molnár, G.; Renz, F.; Kárpáti, S.; Sukla, A.; de Groot, F. M. F. *J. Phys. Chem. B* **2006**, *110*, 11647.
(62) Delgado-Jaime, M. U.; Kennepohl, P. http://www.sourceforge.net/projects/blueprintxas, 2010.

(63) Delgado-Jaime, M. U.; Kennepohl, P. *J. Synchrotron Radiat.* **2010**, *17*, 119.
(64) Delgado-Jaime, M. U.; Dible, B. R.; Chiang, K. P.; Brennessel, W. W.; Bergmann, U.; Holland, P. L.; DeBeer, S. *Inorg. Chem.* **2011**, *50*, 10709.
(65) Neese, F. *J. Biol. Inorg. Chem.* **2006**, *11*, 702.
(66) Römelt, R.; Ye, S.; Neese, F. *Inorg. Chem.* **2009**, *48*, 784.
(67) DeBeer George, S.; Petrenko, T.; Neese, F. *J. Phys. Chem. A.* **2008**, *112*, 12936.
(68) Becke, A. D. *Phys. Rev. A* **1988**, *38*, 3098.
(69) Perdew, J. P. *Phys. Rev. B* **1986**, *33*, 8822.
(70) Perdew, J. P. *Phys. Rev. B* **1986**, *34*, 7406.
(71) DeBeer George, S.; Neese, F. *Inorg. Chem.* **2010**, *49*, 1849.
(72) Delgado-Jaime, M. U.; DeBeer, S. http://www.sourceforge.net/projects/moanalyzer, 2011.
(73) Pangborn, A. B.; Giardello, M. A.; Grubbs, R. H.; Rosen, R. K.; Timmers, F. J. *Organometallics* **1996**, *15*, 1518.
(74) Sur, S. K. *J. Magn. Reson.* **1989**, *82*, 169.
(75) Solé, V. A.; Papillon, E.; Cotte, M.; Walter, P.; Susini, J. *Spectrochim. Acta, Part B* **2007**, *62*, 63.
(76) Webb, S. *SixPACK, SSRL, SLAC*; Stanford University: Stanford, CA, 2010.
(77) Neese, F., *Orca: an ab initio, DFT and Semiempirical Electronic Structure Package*, Version 2.8, Revision 2287; Institut für Physikalische und Theoretische Chemie, Universität Bonn: Bonn, Germany, 2010.
(78) Lee, C. T.; Yang, W. T.; Parr, R. G. *Phys. Rev. B* **1988**, *37*, 785.
(79) Neese, F.; Solomon, E. I. In *Magnetism: From Molecules to Materials*; Miller, J. S., Drillon, M., Eds.; Wiley: New York, 2002; Vol. *4*, p 345.
(80) Schäfer, A.; Horn, H.; Ahlrichs, R. *J. Chem. Phys.* **1992**, *97*, 2571.
(81) Schäfer, A.; Huber, C.; Ahlrichs, R. *J. Chem. Phys.* **1994**, *100*, 5829.
(82) Weigend, F.; Ahlrichs, R. *Phys. Chem. Chem. Phys.* **2005**, *7*, 3297.
(83) Eichkorn, K.; Weigend, F.; Treutler, O.; Ahlrichs, R. *Theor. Chem. Acc.* **1997**, *97*, 119.
(84) Eichkorn, K.; Treutler, O.; Öhm, H.; Häser, M.; Ahlrichs, R. *Chem. Phys. Lett.* **1995**, *240*, 283.
(85) Eichkorn, K.; Treutler, O.; Öhm, H.; Häser, M.; Ahlrichs, R. *Chem. Phys. Lett.* **1995**, *242*, 652.
(86) Neese, F.; Wennmohs, F.; Hansen, A.; Becker, U. *Chem. Phys.* **2009**, *356*, 98.
(87) Kossmann, S.; Neese, F. *Chem. Phys. Lett.* **2009**, *481*, 240.
(88) Neese, F. *J. Comput. Chem.* **2003**, *24*, 1740.
(89) Ginsberg, A. P. *J. Am. Chem. Soc.* **1980**, *102*, 111.
(90) Noodleman, L.; Peng, C. Y.; Case, D. A.; Mouesca, J. M. *Coord. Chem. Rev.* **1995**, *144*, 199.
(91) Kirchner, B.; Wennmohs, F.; Ye, S.; Neese, F. *Curr. Opin. Chem. Biol.* **2007**, *11*, 134.
(92) Neese, F. *J. Phys. Chem. Solids* **2004**, *65*, 781.
(93) *Molekel*, Advanced Interactive 3D-Graphics for Molecular Sciences, available under http://www.cscs.ch/molkel/.
(94) Neese, F. *Inorg. Chim. Acta* **2002**, *337*, 181.
(95) Sinnecker, S.; Slep, L. D.; Bill, E.; Neese, F. *Inorg. Chem.* **2005**, *44*, 2245.
(96) ftp.chemie.uni.-karlsruhe.de/pub/basen
(97) Ahlrichs, R. *and coworkers*, unpublished results.
(98) Sinnecker, S.; Rajendran, A.; Klamt, A.; Diedenhofe, M.; Neese, F. *J. Phys. Chem. A.* **2006**, *110*, 2235.
(99) Pipek, J.; Mezey, P. G. *J. Chem. Phys.* **1989**, *90*, 4916.
(100) Pettersen, E. F.; Goddard, T. D.; Huang, C. C.; Couch, G. S.; Greenblatt, D. M.; Meng, E. C.; Ferrin, T. E. *J. Comput. Chem.* **2004**, *13*, 1605.
(101) *Kaleidagraph: Tools for Discovery*, Version 4.03; Synergy Software: Reading, PA, 1986−2006.
(102) Delgado-Jaime, M. U.; DeBeer, S. *submitted for publication.*